STOCHASTIC NUMERICAL APPROXIMATION APPROACHES FOR ESTIMATION OF TRAFFIC VOLUME UNDER TRAVEL DEMAND UNCERTAINTIES

BY

KUMAR NEELOTPAL SHUKLA

THESIS

Submitted in partial fulfillment of the requirements
for the degree of Master of Science in Civil Engineering
in the Graduate College of the
University of Illinois at Urbana-Champaign, 2017

Urbana, Illinois

Adviser:

Professor Hadi Meidani

Abstract

The traditional deterministic process of trip assignment does not account for uncertainties in traffic demands. These point-estimate based solutions often results in large differences between forecasted and actual traffic volumes thereby imposing huge financial burdens upon development agencies. In this work, stochastic treatment has been given to the trip assignment problem, specifically the network user equilibrium problem solved using the variational inequality method, under demand uncertainties modeled as random inputs. Smolyak sparse grid interpolation technique was successfully applied to the problem and compared to Monte Carlo sampling. Performance of constructed interpolant was evaluated through output distribution recovery , statistical moment estimation, and computation time comparisons. Ability of sparse grid to efficiently handle demand uncertainties using as many as 5 times fewer points than Monte Carlo sampling in pragmatically sized transportation networks was demonstrated.

Keywords: *trip assignment, user equilibrium, variational inequality, smolyak sparse grid, polynomial chaos expansions*

Acknowledgments

I would like to express profound gratitude to my advisor Dr. Hadi Meidani for giving me the opportunity to be a part of this project and all the guidance and support he has given me along the way. I am inspired by the high standards that he sets for himself and those around him, his attention to detail, his dedication to the profession, and his intense commitment to his work. I have thoroughly enjoyed working with him and feel like I have learned a lot.

I would like to give special thanks to my parents, Dr. Mahesh Shukla and Mrs. Alka Shukla, for being incredibly supportive and patient during the course of this MS program and to my friends, Manika, Vaibhav, Rishabh, and Sudipta for reminding me not to work too hard. The four of you have kept my world centered. Special thanks also go to them for teaching me the value of hard work, efficiency, and self-sufficiency.

I could not go without thanking the brains trust whom I sat with and bounced ideas off of on a daily basis. Thank you Negin Alemazkoor and Mohammad Amin Nabian and many others. I also appreciate the great support from the staff at the Newmark Civil Engineering Lab.

Table of Contents

Chapter 1

Introduction

1.1 Uncertainty Quantification

Uncertainty quantification is an amalgam of modern and classic research fields. In a way, it has existed alongside the areas of probability and statistics. The novelty is derived from the recent advent of computational techniques that have supplemented scientific modeling. Researchers develop scientific models with the objective of mimicking physical realities in order to derive knowledge. These models exhibit great diversity in terms of complexity - ranging from simplistic models with one input and one characterizing parameter to highly complex models with numerous inputs and parameters. Two distinct paths exist from reality to knowledge: 1. purely statistical models based on observations of physical reality, and 2. path from reality to mathematical models, calibrated and informed by observations, which are then discretized into numerical models. With the massive increase in computational capabilities and advent of high speed computing, the second path, often referred to as scientific computing, has become the main tool for understanding the many complex engineering phenomena one encounters in the real world [1].

Advantages of scientific computing over experimental studies are twofold: 1. experiments can be expensive, prohibitively time-consuming and in certain cases such as atmospheric sciences near impossible to conduct, and 2. virtual nature of simulations provides great freedom to researchers in terms of parameter and input choices without risk of any harm or injury. This lucrative field remains an active area of research. Researchers aim to develop highly efficient algorithms with controlled numerical errors. However, one common form of oversimplification often encountered in computational modeling is the use of deterministic values for inputs and parameters as it is very well known that the real world is hardly certain.

If we revisit the path from physical reality to knowledge, it can be seen where and how may uncertainty creep into this otherwise highly efficient process. While translating reality

to a tractable mathematical model, one often ends up with simplifying assumptions referred to as *modeling errors*. The inputs themselves may not exactly replicate real life situations and therefore contribute *input uncertainty*. When the mathematical model is converted into a numerical model, since computers only have limited working precision and cannot handle abstract notions such as infinity, *discretization errors* are committed. Three distinct sources of uncertainty are present in this three stage process. However, uncertainty does not necessarily represent a bad thing - it simply is the variation in data which stems from our incomplete understanding of the underlying physics and inevitable measurement errors. Goal of the emerging field of *uncertainty quantification* (UQ) is to quantify this randomness and provide reliable quantitative outputs in its presence. It should also be remembered that the physical world itself is random and therefore incorporation of uncertainty actually improves scientific models by bringing them closer to reality.

1.2 Probability Theory

In order to mathematically quantify variation in data, one must understand the concepts of probability theory.

1.2.1 Probability Spaces

A random variable, $X = X(\omega)$, is a variable whose possible values are numerical outcomes of a random phenomenon where ω belongs to the outcome space Ω, often also referred to as the *sample space*. We further define $\mathcal{F}$, a σ-algebra on Ω, as a collection of all possible subsets of Ω which contains the null set ϕ and is closed under union, intersection and complement operations i.e.

1. It is not empty: $\phi \in \mathcal{F}$ and $\Omega \in \mathcal{F}$
2. If $A \in \mathcal{F}$, then $A^c \in \mathcal{F}$
3. If $A_1, A_2, ... \in \mathcal{F}$, then
$$\bigcup_{i=1}^{\infty} A_i \in \mathcal{F} \quad \text{and} \quad \bigcap_{i=1}^{\infty} A_i \in \mathcal{F}$$

Further, we define a *measure* on a measurable space $(\Omega, \mathcal{F})$ as a function $\mu : \mathcal{F} \to \Re \cup [-\infty, +\infty]$ such that:

1. $\forall A \in \mathcal{F} : \mu(A) \geq 0$
2. $\mu(\phi) = 0$

3. $\mu(\bigcup_{i=1}^{\infty} A_i) = \sum_{i=1}^{\infty} \mu(A_i)$ for all countable collection $\{A_i\}$ of pairwise disjoint sets in $\mathcal{F}$

Then the triplet $(\Omega, \mathcal{F}, \mu)$ is a measure space. A probability space is a measure space where $\mu(\Omega) = 1$.

1.2.2 Distributions

The cumulative distribution function (CDF) $F_X(x)$ is defined as the collection of probabilities

$$F_X(x) = \mu\{\omega \in \Omega : X(\omega) \leq x\}, \quad x \in \Re \tag{1.1}$$

CDF of a random variable provides information about the probability of X belonging to an interval. However, we are often also interested in determining the probability of X being equal to some number or a set. The collection of probabilities

$$P_X(B) = \mu\{\omega \in \Omega : X(\omega \in B)\}, \quad B \subset \Re \tag{1.2}$$

Distributions can either be discrete or continuous. As the name suggests, if a distribution has jumps it is discrete. The associated random variable is referred to as a *discrete random variable*. These assume only finite or countably infinite values $x_1, x_2, ...$ with corresponding probabilities $p_k = \mu(X = x_k)$. Binomial distribution used for reliability analysis via calculation of failure/defect rates on manufacturing shop floors and the Poisson distribution used for earthquake recurrence risk analyses are examples of discrete distributions.

On the other hand, a distribution which does not have any jumps and is relatively 'smooth' is considered continuous. As with the previous case, associated random variables are called *continuous random variables*. The probability of a continuous random variable assuming any particular value is 0 i.e. $\mu(X = x) = 0, \quad \forall x \in \Re$. Continuous distributions are commonly represented by a density f_X:

$$F_X(x) = \int_{-\infty}^{x} f_X(y)dy, \quad x \in \Re \tag{1.3}$$

where

$$f_X(x) \geq 0, \forall x \in \Re \quad \text{and} \quad \int_{-\infty}^{\infty} f_X(y)dy = 1$$

Two most commonly used continuous distributions are the Normal and Uniform distributions. They are both extensively used to represent real-valued random variables with unknown distributions. An important characteristic of the normal (or Gaussian) distribution is the central limit theorem which states that averages of samples of observations of

independent random variables independently drawn converge to the normal distribution if the number of observations is sufficiently large. It is also the maximum entropy distribution i.e. an upper bound uncertainty model when mean and standard deviation are known.

Uniform distribution is another important symmetric continuous distribution. It is constant for all intervals of same length inside its support characterized by a minimum and a maximum value. It is useful when the range of variation is known but no further information is available. Uniform distribution represents the zero information case for bounded supports. It has a density,

$$f_X(x) = \begin{cases} \frac{1}{b-a}, & x \in (a,b) \\ 0, & \text{otherwise} \end{cases} \tag{1.4}$$

1.2.3 Expected Value and Variance

Two important characteristics of a random variable are its *expected value* and *variance*. These are also the most frequently cited *summary statistics*, practically communicable and easily interpretable descriptor values. The expected value or *mean* of the random variable describes its central location and for an R.V. with density f_X is given by:

$$\mathbb{E}(X) = \int_{-\infty}^{\infty} x f_X(x) dx \tag{1.5}$$

Variance describes variability around this central value and is given as:

$$\sigma_X^2 = \text{var}(X) = \int_{-\infty}^{\infty} (x - \mathbb{E}(X))^2 f_X(x) dx \tag{1.6}$$

As it can be seen from the preceding equation, unit of variance is the unit of random variable squared. To get around this issue, *standard deviation*, σ_X, of a random variable is defined as the square root of its variance.

1.2.4 Random Vectors

Let $X_1, X_2, ..., X_n$ be one-dimensional real-valued random variables. The vector $\mathbf{X} : \mathbf{\Omega} \rightarrow \Re^n, \mathbf{X} = [X_1, X_2, ..., X_n]$ is called a *random vector*. Corresponding distribution function known as the *joint CDF* is denoted by $F_{\mathbf{X}} : \Re^n \rightarrow [0,1]$ and is defined by:

$$F_{\mathbf{X}}(x_1, ..., x_n) = \mu(X_j \leq x_j, j = 1, ..., n) \tag{1.7}$$

In case the distribution of a random vector $\mathbf{X}$ has a density $f_{\mathbf{X}}$, the following is true:

$$F_{\mathbf{X}}(x_1, ..., x_n) = \int_{-\infty}^{x_1} \cdots \int_{-\infty}^{x_n} f_{\mathbf{X}}(y_1, ..., y_n) dy_1 \cdots dy_n \tag{1.8}$$

where

$$f_{\mathbf{X}} \geq 0, \forall \mathbf{x} \in \Re \quad \text{and} \quad \int_{-\infty}^{\infty} \cdots \int_{-\infty}^{\infty} f_{\mathbf{X}}(y_1, ..., y_n) dy_1 \cdots dy_n = 1$$

1.2.5 Independence

The last important concept in probability theory necessary to facilitate formulation and discussions in subsequent sections is that of independence. Instinctively, a set of random events are considered *independent* if the outcome of one does not influence the outcomes of others. Mathematically, we can define independence using recently outlined concepts of joint distribution function and densities. Random variables $X_1, X_2, ..., X_n$ are independent if and only if their joint CDF can be written as:

$$F_{\mathbf{X}}(x_1, ..., x_n) = F_{X_1}(x_1) \cdots F_{X_n}(x_n), \quad (x_1, ..., x_n) \in \Re^n \tag{1.9}$$

Alternatively, independence can be defined based on density $f_{\mathbf{X}}$. $X_1, X_2, ..., X_n$ are independent if and only if,

$$f_{\mathbf{X}}(x_1, ..., x_n) = f_{X_1}(x_1) \cdots f_{X_n}(x_n), \quad (x_1, ..., x_n) \in \Re^n \tag{1.10}$$

1.3 Overview of UQ Techniques

The classical approach to understanding the effects of uncertainty on models is through stochastic partial or ordinary differential equations. Random inputs to these are idealized processes such as Poisson process, etc., and tools like stochastic calculus have been developed to solve these equations. This remains an active area of research [2, 3, 4, 5].

Under scientific computing, a different approach is taken for numerical modeling in the presence of uncertainty. Variability in inputs is captured using random variables and the existing deterministic procedures are reformulated as stochastic systems. An overview of methods used for obtaining relevant information from such systems is presented in this section.

The most straightforward class of methods are *sampling based methods*, the most popular being Monte Carlo sampling along with its variants. It provides access to complete statistics of the solution and its convergence performance does not depend upon the number of inde-

pendent random input variables. In this technique, one draws a large number of realizations of the random inputs based on their known distributions. Each realization provides fixed input data which can be used to solve the working deterministic code. A solution ensemble is created from which statistical information can be derived. The biggest drawback of this technique is the 'large number' of realizations - typically hundreds of thousands are required to get meaningful insights. If the deterministic code is computationally intensive, the stochastic version of the problem quickly becomes intractable due to excessive computational burden. Improvements have been made to the traditional brute-force method through techniques like Latin hypercube sampling [6, 7] and quasi-Monte Carlo sampling [8, 9, 10], both of which alleviate some of the classical problems.

Second class comprises of perturbation methods where random fields are expanded via Taylor series around their mean and truncated at a certain order. Despite extensive usage in various engineering fields [11, 12, 13], these methods suffer from a serious drawback - their performance is limited by the extent of variability in input data, with typical upper bound being approximately 10%.

Two more classes of techniques are *moment equations* and *operator-based methods*. In the former, attempts are made to directly calculate moments of the random solution via averaging original stochastic governing equations. Primary challenge in using this technique is the closure problem - calculating a moment often requires higher moments to already be known. The latter class is based on manipulation of stochastic operators present in the governing equations. Two techniques from this class are Neumann expansion [14] and the weighted integral method [15, 16, 17]. They suffer from the same drawback as perturbation methods i.e. limit on uncertainty in input data. Further, their performance is also strongly dependent upon the underlying operator.

A more recently developed class is the *generalized polynomial chaos* (gPC) category. These are essentially surrogates that approximate the output, or Quantity of Interest (QoI), as a polynomial function in the random space of parameters [18]. This approach is based on the spectral stochastic finite element method. The fundamental notion is projection of dependent variables of the model onto a random space spanned by orthogonal polynomials to obtain a polynomial expansion which can then be employed as a surrogate. The expansions can then be used for replacing computationally expensive and temporally limiting full-scale model simulations for engineering procedures [19] [20] [21]. The original work on polynomial chaos [22], Gaussian random variables were used with Hermite polynomials as basis functions. To improve convergence and facilitate probability approximations for non-Gaussian problems, the scheme was extended to include other random distributions resulting in generalized polynomial chaos expansions (gPC), hereafter referred to as polynomial chaos

expansions (PCE) [23]. A series of works demonstrate the successful application polynomial chaos methods to uncertainty propagation in a variety of applications [24, 25, 26, 27]. Convergence studies [ernst] have shown that methods of this category exhibit fast convergence if optimal selection of basis functions is made. Challenges were encountered in case of discontinuous dependence on inputs. This issue was alleviated and the assumption of global smoothness relaxed via development of efficient and robust schemes, further generalizing PCE to include piecewise polynomial bases [28].

Another attractive alternative to the spectral techniques discussed in the preceding paragraph is the *stochastic collocation* method. One repeatedly evaluates the deterministic code at predetermined set of realizations in the random space defined by random inputs.This class includes sparse grid [20] and newly developed adaptive sparse grid interpolation [29] that incorporate intelligent sampling of inputs. Most early works are more suited to problems with solutions having regular dependence on input random variables. In such cases, very fast convergence can be obtained using orthogonal tensor products of polynomials. However, these methods are only suitable for problems with a small number of independent random variables since they suffer from the *curse of dimensionality*. The number of evaluation nodes grows exponentially with the number of independent random variables. Therefore, even with current computational capabilities it is very difficult to evaluate systems containing more than 4 or 5 independent random variables. Smolyak proposed a sparse tensor product which does not scale as poorly as full tensor product and therefore, should be considered when the number of input random variables is large [30]. This method significantly reduces the number of collocation points allowing efficient and accurate approximations, consistent with Monte Carlo estimates using much fewer realizations under certain circumstances. Consequently, the sparse grid method, both in its original [31] [32] [33] and advanced adaptive versions [29], has extensively been applied to engineering problems.

Techniques belonging to the last two classes have the benefit of being non-intrusive i.e. stochastic treatment only requires multiple evaluations of the deterministic counterpart, without any changes to the code or model itself. This is highly advantageous in areas where extensive research has been performed to develop efficient deterministic solution methods, as is the case with network user equilibrium assignment [34] [35].

1.4 Project Motivation

Enormous sums of money get spent on transportation infrastructure projects. The Congressional Budget Office reports that just in the year 2014, public spending on transportation infrastructure was $279 billion. Of this, $165 billion was spent on highways, which encom-

pass both interstate and local roads [36]. Naturally, the financial viability of these projects depends heavily on forecasted traffic volumes [37]. Despite this, 25% of road projects have a difference between actual and forecasted traffic of more than ±40% [38]. It has been found that a major source of this problem are the uncertainties involved in trip generation, the first step of a 4-step Urban Transport Planning System (UTPS) travel demand modeling process involving trip generation, trip distribution, mode split, and trip assignment. Each of these steps may be carried out using one of many available techniques.

The current work focuses on the last stage i.e. trip assignment and the associated user equilibrium (UE) technique. This technique utilizes an iterative process to obtain equilibrium traffic flows throughout the network such that no traveler can reduce his/her travel time by switching routes. Two key inputs to any method within this technique class are 1. the trip table, obtained after the mode split stage in UTPS, and 2. the transportation network itself, with information including topology as well as travel costs for each road i.e. edge in the network. A user equilibrium problem needs to be resolved for every unique combination of these two inputs.

This brings us to discussion about the second input - the transportation network. Urban planners often have the need to examine various different combinations of a transportation network. This can either be for creating an entirely new network or, more commonly, to evaluate effects of altering the configuration of an existing network in an optimal manner - commonly referred to as the *Network Design Problem* (NDP). Formally, it can be defined as an optimization problem with an objective to optimize a system performance measure such as total travel cost while accounting for user route choice behaviors [39]. Consisting of two components - a discrete edge additional problem and a continuous capacity expansion form, the NDP is one of the most challenging transportation problem and remains an active area of research. Researchers have employed various numerical techniques and mathematical formulations in their solution attempts. Some examples include [40], simulated annealing approach using variational inequality formulation [41], bilevel linear programming [42], and nonlinear optimization solved using direct search [43]. Stochastic versions of the NDP with uncertain travel demand have also been solved using probabilistic variations of aforementioned techniques [44, 45].

However, in practice the most common method of network design is to specify multiple configurations and analyze them individually [43]. Most probable reason for this is the widespread availability of traffic assignment codes [46, 47, 48, 49] contrasted against the limited number of optimization codes for large networks. Additions and removals of roads, road capacity changes, directional modifications such making a road one-way, all classify as configuration changes. The UE problem has to be resolved for each new configuration. If

the trip table also happens to be uncertain, the number of UE evaluations quickly become large.

Traditionally, Monte Carlo methods have been used to tackle travel demand uncertainties [50]. Recently, genetic algorithms have also been used to approach this issue [51]. In either case, a large number of samples are required to accurately estimate mean traffic volumes on each edge. As a direct consequence, the computational time required by these methods is high. This problem is further exacerbated by the fact that a new UE solution needs to be obtained for all configurations considered by planners.

The objective of this study is to apply the techniques of sparse grid interpolation and polynomial chaos expansion in order to rapidly obtain estimates of traffic volumes on a pragmatically sized transportation network.

1.5 Background

1.5.1 Demand Uncertainties

There exists potential for introduction of uncertainty in each of the 4 sequential steps of the UTPS process. Sources and brief descriptions for these hav been provided below:

1. **Trip generation** predicts traffic volumes generated and attracted to each zone within a network. Predictions are based on socioeconomic variables such as household incomes, auto ownership and size, zonal employment levels, and accessibility of the zone in terms of distance. The Institute of Transportation Engineers' (ITE) *Trip Generation* manual, one of the most widely used references for determining trip rates, provides vehicle trip rates for different land use classes [52]. Alternatively, regression and cross-classification models are also used which exploit correlations between previously mentioned socioeconomic variables and trips. There are several sources of uncertainty in both models - regression uses "best-fit" equations to determine variable coefficients whereas the trip production and attraction rates in cross-classification models can be considered uncertain.

2. **Trip distribution** links the trip ends predicted by trip generation to form origin-destination (OD) pair flows. Final outcome of this step is a trip-table, which contains traffic demand estimates between each origin and destination in the network. The most commonly used model for trip distribution is the gravity model [52]. Inputs to this model are total numbers of trips produced by a certain origination zone i, total number of trips attracted to destination zone j, and an impedance function representing travel

cost between zones i and j. Gamma, power, or exponential functions are typically used and their parameters can be uncertain.

3. **Mode split** predicts the percentages of travel flow between each OD pair which may use the different modes available - most commonly transit or auto. These percentage splits cannot be accurately predicted and therefore, are uncertain.

4. **Trip Assignment** assigns paths through the network to demands between each OD pair. All-or-nothing and capacity-restrained are two major classes of methods used for trip assignment. User equilibrium is a capacity-restrained method which has been found to reduce uncertainties propagated through previous steps. While precise reasons are unknown, it has been suggested that equilibrium assignment is very stable for a network with well-defined constraints [53].

Since trip assignment *assigns* traffic flows to edges in the network, uncertainties of the first three steps combined are referred to as demand uncertainties. As previously pointed out, there can be several reasons behind demand uncertainties. Coefficients from regression analysis need not necessarily explain all observations - they only represent the "best-fit", trip generation and attraction rates cannot be accurately estimated to one value with zero variation in real-life scenarios, and nor can modal split be perfect. A model validation step is recommended to satisfactorily determine and confirm if forecasts match actual demands. However, a major criticism is the general lack of effort put into validation because of time, budget and data constraints [52]. Further, validation only assesses predictive strength for the contemporary scenario. Future erratic behavior of forecasts, stemming from systemic uncertainties, cannot be assessed or bounded by model validation [50].

For most analyses, variations in parameter estimates, even if observed, are not reported. As a result, the entire UTPS traffic volume forecast process relies on point estimates, typically means [50]. Neglect in conveying uncertainty damages the reliability of traffic estimates and ultimately lead to cost overruns. Overestimation of traffic volumes leads to unused roads whereas underestimation of volumes leads to under-dimensioning and future changes in capacity of operational roads, which is even costlier. Therefore, it is absolutely necessary to obtain robust traffic volume forecasts under demand uncertainties in order to reduce financial and operational risks.

These uncertainties can be adopted to mathematical systems via probabilistic settings in case enough information is available to characterize them. In this case, they are modeled as *random variables*. Particularly, since mean estimates of demand are conveyed and used for traffic estimation in contemporary practice, demands can be modeled as uniform random variables with specified means. Distributions centered around these means can be

constructed based on the extent of variability. The following mathematical and computational analysis aims to obtain complete statistical information about the output given the uncertain inputs are adequately characterized. Therefore, the *Quantity of Interest (QoI)* is the complete distribution of traffic volume on a selected edge.

In a realistic setting, while some demands may be very accurately estimated, some might have uncertainties associated with them because of one or more of the previously stated reasons. It is possible that demand between specific OD pairs cannot be quantified with high levels of accuracy and are considered uncertain. They may not have any correlation structure with other demands originating/terminating from the same node. Uncertain demands can therefore be considered independent of each other ,and modeled as i.i.d. uniform random variables.

Chapter 2

Problem Formulation

2.1 User Equilibrium

Mathematical formulations largely depend upon the associated final use cases. Two comprehensive and easy-to-understand formulations have been offered by [54] and [55]. Former was used for providing theoretical proofs of solution existence and development of solution methodology for the variational inequality process for solving traffic user equilibrium. Latter was used for development of a reduction technique that employs the variational inequality process and applies it to traffic networks with uncertain parameters including travel demands and edge costs. owing to similarity in application, the second option has been largely adopted with minor modifications for use in this work.

Consider a transportation network consisting of a finite set of nodes $n \in N$ and directed edges $i \in E$. These nodes form origin-destinations pairs $(k, l) \in P \subseteq N^2$. Traffic demand between each pair *(k,l)* is represented as $d_{k,l} \in \Re^+$ where $\Re^+$ represents non-negative real numbers. Each pair *(k,l)* is connected by a finite non-empty set of routes $r \in R_{k,l}$, each a string of edges representable as a binary column vector $\Delta_r = (\Delta_{ir} : i \in E)$ with $\Delta_{ir} = 1$ if edge e is part of route r, and 0 otherwise. Traffic volume flow on an edge i is given by $q_i \in \Re^+$.
To satisfy the conservation of flow, the following condition must be met:

$$\mathbf{A}\vec{q} = \vec{b} \tag{2.1}$$

where $\vec{q}$ is the vector of all volume flows, $\vec{b}$ is the vector of demands such that $b_i = \sum_j d_{ij}$,

and $\boldsymbol{A}$ is a matrix such that:

$$A_{ij} = \begin{cases} 1, & \text{if edge } j \text{ originates at node } i \\ -1, & \text{if edge } j \text{ terminates at node } i \text{ and } \sum_j d_{ij} = 0 \\ 0, & \text{otherwise} \end{cases} \tag{2.2}$$

A function $c : \Re^+ \to \Re^+$ is an edge-cost function where $c(q) = (c_i(q) : i \in E)$ is the vector of cost per unit traffic volume for each edge i. For each route, $r \in R$, route cost is the aggregate of its edge costs, i.e.

$$c_r(q) = \Delta_r^T c(q) \tag{2.3}$$

If the minimum route cost for each $q \in \Re^+$ and $(k, l) \in P$ is denoted by

$$c_{k,l}(q) = \min\{c_r(q) : r \in R_{k,l}\} \tag{2.4}$$

then the edge flow vector, $\vec{q^*}$ is defined as the network user equilibrium condition *(c,**D**)* for a given edge cost function, c, and travel demand matrix, $\mathbf{D} = [d_{k,l}], 1 \leq k, l \leq |N|$, iff for each $r \in R_{k,l}$ and $(k, l) \in P$, the following condition is satisfied.

$$c_p(q^*) = c_{k,l}(q^*) \tag{2.5}$$

The vector, q^*, is designated as the equilibrium edge-flow vector. In an original approach, [54] suggested the equilibrium edge flows for a cost-demand combination, *(c,**D**)*, can be obtained as a solution to a variational inequality problem. In a general sense, the finite dimensional variational inequality problem defined by function F and non-empty set K, *VI(F,K)* is to determine a vector $x^* \in K \subset \Re^n$, such that

$$F(x^*)^T.(x - x^*) \geq 0, \quad \forall x \in K \tag{2.6}$$

If we define f as a set of feasible edge flows for a given demand matrix, $\boldsymbol{D}$, then for any edge-cost function, c, the solution to *VI(c,f)* exactly corresponds to the equilibrium edge flow vector for network user equilibrium *(c,**D**)*.

2.2 Sparse Grid Collocation

A proportion of travel demands are to be modeled as random inputs. Consider a finite set of nodes $O_{uncertain} \subset N$ representing random origins and another finite set $D_{uncertain} \subset N$ representing random destinations. If the cardinalities of $O_{uncertain}$ and $D_{uncertain}$ are denoted

respectively by $\upsilon_O = |O_{uncertain}|$ and $\upsilon_D = |D_{uncertain}|$, the resultant $\upsilon_O \upsilon_D$ O-D pairs between these nodes are termed as uncertain OD pairs. Formally, let the random traffic demand inputs between these pairs be denoted by a $(\Upsilon = \upsilon_O \upsilon_D)$-dimensional vector, $\mathbf{Z} = (Z_1, ..., Z_\Upsilon) \in \Re^\Upsilon, \Upsilon \geq 1$ of uniform random variables with mutually independent components and a joint probability density function denoted by $\rho(\boldsymbol{\xi})$. The random vector is defined in the probability space $(\Omega, \mathcal{F}, \mu)$, where Ω is the sample space, $\mathcal{F}$ is the corresponding σ-algebra on Ω, and μ is the associated probability measure. Let $\rho_i(\xi_i) \sim \mathcal{U}(0.5 d_{base,i}, 1.5 d_{base,i})$, where d_{base} is nominal value, be the probability densities for Θ_i, and Ω_i the corresponding samples spaces such that

$$\rho(\boldsymbol{\xi}) = \prod_{i=1}^{\Upsilon} \rho_i(\xi_i), \tag{2.7}$$

$$\Omega = \prod_{i=1}^{\Upsilon} \Omega_i \tag{2.8}$$

Let $\Theta_M = \{Z^{(j)}\}_{j=1}^M \subset I_Z$ be a prescribed set of realizations, also called nodes or *collocation points*, in random space, where $M \geq 1$ is the number of points, and $VI(c, f(Z^{(j)}))_{j=1}^M$ be the corresponding solutions to user equilibrium problem. We then need to find numerical approximations, $w(Z) \subset \Pi(Z)$, to the true solution in proper polynomial space $\Pi(Z)$ in the sense that $\|w(Z) - VI(c, f(Z))\|$ is sufficiently small in strong norm defined on I_Z i.e.,

$$\|w(Z) - VI(c, f(Z))\| \to 0, \quad M \to \infty \tag{2.9}$$

In the 1-dimensional case ($\Upsilon = 1$), the following approximation can be considered to interpolate the smooth operator $VI : [0,1]^\Upsilon \to \Re$:

$$\mathcal{U}^i(VI) = \sum_{j=1}^{m_i} VI(\cdot, f(Z_i^{(j)})) \cdot a_i^j \tag{2.10}$$

by using the distinct points from the set

$$\Theta^i = \{Z_i^{(j)} | Z_i^{(j)} \in [0,1] \text{ for } j = 1, ..., m_i\} \tag{2.11}$$

where $i \in \mathbb{N}, a_i^j \equiv a_i(Z_i^{(j)})$ are interpolation nodal basis functions, and m_i is the number of elements in the set Θ^i. The straightforward approach to interpolate over the entire space I_Z in the multivariate case ($\Upsilon > 1$) is to use tensor product,

$$(\mathcal{U}^{i_1} \otimes \cdots \otimes \mathcal{U}^{i_\Upsilon})(VI) = \sum_{j_1=1}^{m_1} \cdots \sum_{j_\Upsilon=1}^{m_\Upsilon} VI(\cdot, f(Z_{i_1}^{(j_1)}), ..., f(Z_{i_\Upsilon}^{(j_\Upsilon)})) \cdot (a_{i_1}^{j_1} \otimes \cdots \otimes a_{i_\Upsilon}^{j_\Upsilon}) \tag{2.12}$$

where the total number of points is $M = m_1 \times \cdots \times m_\Upsilon$, which grows very fast for large Υ making it computationally intractable since each point requires a full evaluation of the underlying deterministic code. That is to say, this approach suffers from the well known *curse of dimensionality*. An alternative approach is the Smolyak *sparse* grid interpolant $\mathcal{A}_{l,\Upsilon}$, originally introduced in [30], which by construction are a product of 1D interpolants, form a subset of the full tensor product, and take the following form [56]:

$$\mathcal{A}_{l,\Upsilon} = \sum_{l-\Upsilon+1 \leq |\mathbf{i}| \leq l} (-1)^{l-|\mathbf{i}|} \cdot \binom{\Upsilon - 1}{l - |\mathbf{i}|} \cdot (\mathcal{U}^{i_1} \otimes \cdots \otimes \mathcal{U}^{i_\Upsilon}) \tag{2.13}$$

where $l \geq \Upsilon$ is the *level* of construction and $|\mathbf{i}| = i_1 + \cdots + i_\Upsilon$ where $\mathbf{i}$ is the multi-index with each $i_k, k = 1, ..., \Upsilon$ representing the level of interpolation along the k^{th} dimension. In order to compute the interpolant, the deterministic model needs to be evaluated at each point of the final set,

$$\Theta_M = \bigcup_{l-\Upsilon+1 \leq |\mathbf{i}| \leq l} (\Theta^{i_1} \times \cdots \times \Theta^{i_\Upsilon}) \tag{2.14}$$

In order to minimize the total number of points, it is intuitive to construct one-dimensional point sets such that they are *nested* i.e.,

$$\Theta^i \subset \Theta^j, \quad i < j \tag{2.15}$$

A popular choice for point sets is the non-equidistant Clenshaw-Curtis grid which represent Chebyshev polynomial extrema [57]. For any i,number of points m_i and the set $\Theta^i = \{Z_i^{(1)}, ..., Z_i^{(m_i)}\}$ are defined as,

$$m_i = \begin{cases} 1, & \text{if } i = 1 \\ 2^{i-1} + 1, & \text{if } i > 1 \end{cases} \tag{2.16}$$

$$Z_i^{(j)} = \begin{cases} -\cos \frac{\pi(j-1)}{m_i - 1}/2, & \text{for } j = 1, ..., m_i, m_i > 1 \\ 0.5, & \text{if } m_i = 1 \end{cases} \tag{2.17}$$

Due to the doubling of nodes with each increasing level, it can be seen that the resulting grid is nested, $\Theta^l \subset \Theta^{l+1}$. As for the 1D basis functions, the piecewise linear hat function has been chosen due to its local support which assists in resolving discontinuities in space

[32]. Any arbitrary a_i^j with local support can be generated as follows:

$$a_i^j = \begin{cases} 1 - (m_i - 1) \cdot |Z - Z_i^{(j)}|, & \text{if} |Z - Z_i^{(j)}| < 1/(m_i - 1) \\ 0, & \text{otherwise} \end{cases} \tag{2.18}$$

where $j = 1, ..., m_i$. The multi-dimensional piecewise linear basis functions can be constructed using tensor product of the 1D functions defined in equation 2.18 as follows:

$$a_{\mathbf{i}}^{\mathbf{j}} = a_{i_1}^{j_1} \otimes \cdots \otimes a_{i_\Upsilon}^{j_\Upsilon} = \prod_{k=1}^{\Upsilon} a_{i_k}^{j_k} \tag{2.19}$$

where each element of the multi-index $\mathbf{j} = \{j_k\}_{k=1}^{\Upsilon}$ represents the position of support point along the k^{th} direction.

2.3 Polynomial Chaos Expansion

If we define a inner product for continuous cases in weighted L2 space, $L_\mu^2(\Omega) = \{f : \Omega \to \Re | \int_\Omega f^2(\boldsymbol{\xi})\mu(\boldsymbol{\xi})d\boldsymbol{\xi} < \infty\}$ as

$$\langle u, v \rangle_\mu = \int_\Omega u(\boldsymbol{\xi})v(\boldsymbol{\xi})\mu(\boldsymbol{\xi})d\boldsymbol{\xi} \tag{2.20}$$

then one can introduce a system of one-dimensional polynomials $\{\psi_{a,i}(\xi_i)\}, a \in \mathbb{N}_0$ that satisfy the orthogonality relations

$$\langle \psi_{m,i}, \psi_{n,i} \rangle_\mu = \gamma_n \delta_{mn} \quad \forall\, m, n \in \mathbb{N}_0 \tag{2.21}$$

$$\gamma_n = \langle \psi_{n,i}, \psi_{n,i} \rangle_\mu = \|\psi_{n,i}\|_\mu^2 \quad \forall\, n \in \mathbb{N}_0 \tag{2.22}$$

where $\delta_{mn} = 0 \quad \text{if} \quad m = n$ and $\delta_{mn} = 1 \quad \text{if} \quad m \neq n$ is the Kronecker delta function and $\mathbb{N}_0 = \mathbb{N} \cup 0$. The type of polynomial depends upon the probability density $\rho_i(\xi_i)$. For example, Legendre polynomials are used if $\rho_i(\xi_i)$ follows a uniform distribution, as in this case. The multidimensional orthonormal polynomials are obtained from tensorization of one-dimensional polynomials as follows:

$$\psi_{\mathbf{m}}(\boldsymbol{\xi}) = \psi_{1,1}(\xi_1)...\psi_{\Upsilon,\Upsilon}(\xi_\Upsilon), \quad \mathbf{m} = (m_1, ..., m_\Upsilon) \tag{2.23}$$

And therefore,

$$\langle \psi_{\mathbf{n}}(\boldsymbol{\xi}), \psi_{\mathbf{m}}(\boldsymbol{\xi}) \rangle_{\mu} = \|\psi_{n,i}\|_{\mu}^{2} \delta_{\mathbf{mn}}, \quad \forall\, \mathbf{m}, \mathbf{n} \in \mathbb{N}_{0}^{d} \tag{2.24}$$

For an edge i under consideration and a fixed cost function c, the Quantity of Interest (QoI) viz. equilibrium traffic volume flow q_i^* can be represented as a solution to $VI(c, f(Z))$ for each realization of the demand vector Z

$$q_i^* \subset q^* = VI(c, f(\mathbf{Z})) \tag{2.25}$$

We then use our construction to approximately represent the square-integrable function $VI(c, f(\mathbf{Z})) : \Omega \to \Re$ as a finite order truncated polynomial chaos (PC) expansion:

$$VI_k(c, f(Z)) := \sum_{\mathbf{a} \in \Lambda_{\Upsilon,k}} y_{\mathbf{a}} \psi_{\mathbf{a}}(Z) \tag{2.26}$$

where $\{\psi_{\mathbf{a}}, \mathbf{a} \in \mathbb{N}_0^d\}$ is a set of orthogonal basis functions which satisfies equation 2.24, k is the total order of the PC expansion, and $\Lambda_{\Upsilon,k}$ is the set of multi-indexes defined as

$$\Lambda_{\Upsilon,k} = \{\mathbf{a} \in \Lambda_{\Upsilon,k} : \|\mathbf{a}\|_1 \leq k\} \tag{2.27}$$

i.e. a multi-dimensional PC expansion with order k includes multi-dimensional polynomials with order less than or equal to k. The cardinality of $\Lambda_{\Upsilon,k}$, denoted by K, is given by

$$K := \Lambda_{\Upsilon,k} = \frac{(\Upsilon + k)!}{\Upsilon! k!} \tag{2.28}$$

A PC surrogate is constructed by calculating the coefficients, $\mathbf{y} = (y_1, ..., y_K)^T$, in equation 2.26 using M realization sets of random vector $\mathbf{Z}$,$\{Z^{(i)}\}_{i=1}^{M}$, and corresponding QoI samples denoted by vector $\mathbf{u} = (VI(c, f(Z^{(1)})), ..., VI(c, f(Z^{(M)})))$. In availability of these input-output tuples, the coefficients can be obtained as solution to the following system of equations:

$$\mathbf{\Phi y} = \mathbf{u} \tag{2.29}$$

where $\mathbf{\Phi}$ is the measurement matrix constructed according to the following procedure:

$$\mathbf{\Phi} = [\phi_{ij}], \quad \phi_{ij} = \phi_{a^j}(Z^{(i)}), \quad 1 \leq i \leq M, \quad 1 \leq j \leq K \tag{2.30}$$

This system has a unique solution in exact, $M = K$, and overdetermined, $M > K$, cases in a least squares sense which minimizes residual in the latter.

Chapter 3

Approach

3.1 User Equilibrium

Solution approach adopted for solving the user equilibrium traffic assignment problem is the variational inequality technique, as originally suggested by [54]. In development of this algorithm, Dafermos has performed rigorous theoretical treatment including discussions on the existence and uniqueness of the user equilibrium. It is an iterative procedure in which the number of iterations can be known a priori for any given accuracy of result. The technique iteratively creates quadratic programs with standard network flow conservation constraints listed in equation 2.2. Solutions to these quadratic systems, which can be obtained using any of the existing algorithms [58] [59] [60], finally converge to the user equilibrium traffic assignment for all edges in the network. Two key selections to be made for the variational inequality procedure are 1. tolerance, arbitrarily set as 1 here, and 2. a symmetric positive definite matrix $\boldsymbol{G}$ of size equal to the number of edges in the network. A typical choice is a diagonal matrix of travel cost coefficients for all edges, which has been used here.

3.2 Sparse Grid Collocation

Second stage was to add germs to the problem. This was done in 3 incremental steps. A set $O_{uncertain} = \{9, 10, 11, 13, 15, 19, 23, 24\}$ of 8 origins and $D_{uncertain} = \{2, 3, 4, 8, 13, 15, 18, 19\}$ of 8 destinations was randomly selected. The resultant O-D pairs between these nodes are considered to have uncertain traffic demand. For the first step, the first 4 entries of both sets were considered, followed by first 6 entries of both, and finally complete sets were considered. This resulted in 16, 36, and 64 *uncertain* O-D pairs, respectively. Nominal values for these demands have been taken from the original network data source and are represented as D_{base}.

The uncertain demands have been modeled as uniform random variables with 50% variation about the nominal value.

$$D_{uncertain} \sim \boldsymbol{U}(0.5D_{base}, 1.5D_{base}) \tag{3.1}$$

Next stage was to draw random samples for a Monte Carlo analysis [61]. This technique has the advantage of being dimension independent and simple. Procedure involves drawing a large number,M_{mc}, of independent realizations from all identically distributed uncertain travel demands, $\{Z^{(i)}\}_{i=1}^{M_{mc}}$. The deterministic network user equilibrium problem is solved at each point $i = 1, ..., M_{mc}$ to obtain solution ensemble $\{q_{mc}^{(i)}\}$. We are interested in distribution of traffic flow on an edge under consideration which can then be recovered from a frequency plot, such as histogram, of $\{q_{mc}^{(i)}\}_{i=1}^{M_{mc}}$. An important decision to be made is the number of samples to be drawn i.e. M_{mc}. This was achieved via setting a termination condition. The process was set to stop when the Monte Carlo error estimate fell below 0.1% of the nominal traffic volume on the edge under consideration. At this stage, the Monte Carlo estimate was considered to have *converged*. These values are taken as ground truth. Typically, for edges with non-linear flows, $\mathcal{O}(10^4)$ samples were required.

The final stage was the sparse grid interpolant construction and evaluation. Since all problems were high dimensional, level of the sparse grid was set to 2. Problems quickly became intractable at higher levels with number of grid points,M, exceeded $\mathcal{O}(10^5)$. Three separate analyses were performed in this stage:

1. Both mean and standard deviation estimates were compared to Monte Carlo values. Since the total number of points required by sparse grid, M, are several times lower than required for Monte Carlo convergence, M_{mc}, comparison between the two has been made at M points. Statistical estimates calculated using both methods have been compared against true values obtained at Monte Carlo convergence. Two terms are employed in quantifying errors in the mean and standard deviation estimates. $\epsilon_{\bar{q},mc}$ represents the absolute difference between mean traffic flow estimates obtained using Monte Carlo sampling with M points and the full set of M_{mc} points. $\epsilon_{\sigma,mc}$ represents the corresponding difference in the standard deviation estimate. The two can formally be defined as,

$$\epsilon_{\bar{q},mc} = \left| \frac{1}{M_{mc}} \sum_{j=1}^{M_{mc}} q_{mc}^{(j)} - \frac{1}{M} \sum_{j=1}^{M} q_{mc}^{(j)} \right| \tag{3.2}$$

$$\epsilon_{\sigma,mc} = \left| \sqrt{\frac{1}{M_{mc}-1} \sum_{j=1}^{M_{mc}} (q_{mc}^{(j)} - \overline{q_{mc}})^2} - \sqrt{\frac{1}{M-1} \sum_{j=1}^{M} (q_{mc}^{(j)} - \overline{q_{mc}})^2} \right| \tag{3.3}$$

2. The constructed sparse grid interpolant, $\mathcal{A}_{l,\Upsilon}$, was evaluated at a large number, M_t, of input sample points in order to recreate full distributions of traffic volumes on the edge of interest. 100,000 randomly generated points have been used for the analysis. The results have been stored as the ensemble $\{q_{sg}^{(i)}\}_{i=1}^{M_t}$. With both Monte Carlo and sparse grid solution vectors generated, two more error terms can now be introduced. $\epsilon_{\bar{q},sg}$ represents the absolute difference between mean traffic flow estimates obtained using Smolyak sparse grid interpolant constructed using M points and evaluated at M_t points, and Monte Carlo sampling with full set of M_{mc} points. $\epsilon_{\sigma,mc}$ represents the corresponding difference in the standard deviation estimate. Formal definitions of these are as follows:

$$\epsilon_{\bar{q},sg} = \left| \frac{1}{M_{mc}} \sum_{j=1}^{M_{mc}} q_{mc}^{(j)} - \frac{1}{M_t} \sum_{j=1}^{M_t} q_{sg}^{(j)} \right| \tag{3.4}$$

$$\epsilon_{\sigma,sg} = \left| \sqrt{\frac{1}{M_{mc}-1} \sum_{j=1}^{M_{mc}} (q_{mc}^{(j)} - \overline{q_{mc}})^2} - \sqrt{\frac{1}{M_t-1} \sum_{j=1}^{M_t} (q_{sg}^{(j)} - \overline{q_{sg}})^2} \right| \tag{3.5}$$

All four error terms have been plotted against the number of points in order to depict Monte Carlo convergence and perform visual comparison between performances of the two methods. Additionally, normalized histograms and kernel density estimates [62] of the two solution ensembles have been plotted.

3. Functional relationship of traffic volume, the output, with uncertain travel demands, the inputs, have been explored. For this purpose, a specific input $Z^{(i)}$ is gradually varied over its entire support, $I_{Z^{(i)}}$, in steps of size 0.005 which represents 5 vehicles. All other inputs $Z^{(j)}, j \neq i$ are randomly sampled. For each value of $Z^{(i)}$, 5,000 of sets $\mathbf{Z}$ are used and the outputs aggregated to obtain mean and standard deviation, which are then plotted against $Z^{(i)}$.

Additionally, another metric *time ratio* was introduced to quantify reduction in computational effort achieved through utilization of Smolyak's sparse grid technique. Time ratio, τ, is defined as the ratio of computational time required by Monte Carlo analysis to converge, to the computational time required to construct the sparse grid interpolant. A machine with 2.6 GHz Intel Core i5 processor and 8 GB 1600 MHz DDR3 memory running MATLAB R2016b on macOS Sierra version 10.12.5 was used for the experiments. Openly available package, the Sparse Grid Interpolation Toolbox [63] [64], was used for constructing and evaluating the interpolant $\mathcal{A}_{l,\Upsilon}$.

3.3 Polynomial Chaos Expansion

The same sets $O_{uncertain} = \{9, 10, 11, 13, 15, 19, 23, 24\}$ of 8 origins and $D_{uncertain} = \{2, 3, 4, 8, 13, 15, 18, 19\}$ of 8 destinations have randomly been used. The travel demands have also been modeled in exactly the same manner i.e. as uniform random variables with 50% variability about the nominal value.

500,000 realizations were used to obtain Monte Carlo estimates in this case, which was considered ground truth in the absence of real truth data.

A 64 dimensional second order PCE surrogate was then constructed using this data and coefficients for each of the 2,145 expansion terms were calculated using the linear least squares technique. A subspace trust-region method based on the interior-reflective Newton method described in [58] was used to solve the unconstrained linear least squares system.

Followed by this, multiple surrogates were created using different sample sizes and locations for the training data. The surrogates were constructed using the greedy algorithm for dimensionality reduction developed by [65].This iterative algorithm starts with dimension 1 and order 2, trying to identify the most important dimension based on sparsity of the coefficient vector at each stage. With each iteration, the algorithm adds either a dimension or increases order of the existing surrogate till the end condition is met and sparsity of solution cannot be improved further beyond specified error tolerance. Training data included samples of 3 different sizes $\{100, 300, 500\}$, obtained from 5 different locations for each size. Two error threshold values of 10^{-2} and 10^{-3} were tested as an input parameter to the dimension reduction algorithm. Each surrogate was evaluated via cross-validation on testing data containing 100 samples. In addition to visual evaluation using diagonal plots and histograms, cross-validation performance of different surrogates was also evaluated using L2-norm of normalized vector of estimated values i.e.

$$\epsilon = \| \frac{vol_{PCE} - vol_{true}}{vol_{true}} \|_2 \tag{3.6}$$

where vol_{PCE} is the vector of traffic volume estimates obtained using PCE surrogate and vol_{true} is the vector containing actual traffic volumes obtained via the solution to network user equilibrium problem.

Chapter 4

Case Study: Sioux Falls

4.1 Network Details

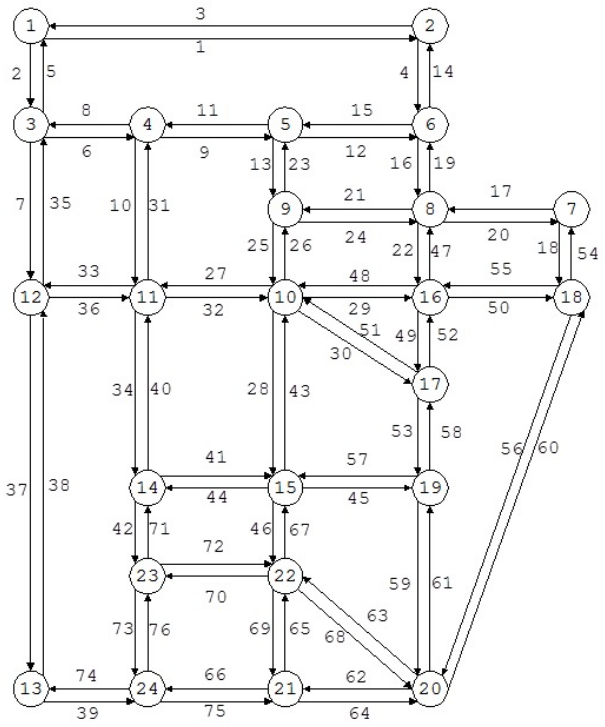

Figure 4.1: Sioux-Falls network.

The methodology has been tested on the mid-sized Sioux Falls network, which has been extensively used by researchers for transportation problems including traffic assignment [66] [67] [68]. The network, shown in figure 4.1, is a simplified representation of the city of Sioux Falls, the largest city in the US state of South Dakota. It consists of 24 nodes connected by

76 directed edges, allowing us to demonstrate the working of developed methodology on a realistically sized network. Travel cost function for edges is the commonly used Bureau of Public Roads'(BPR) link performance function given by:

$$t = t_f \left[1 + b\left(\frac{q}{q_{max}}\right)^p\right] \tag{4.1}$$

where t is travel time (in minutes) on the edge, t_f is the free flow time (in minutes), q is volume flow, q_{max} is capacity, b and p are volume delay parameters. The traditional BPR value of $b = 0.15$ has been used for the network and $p = 4$ for all edges. Best-known link flow solutions, obtained from [66], have been used as starting guess for all implementations to ensure consistency between outputs.

Two roads, edges 26 and 32, have been selected for analysis and results presented in the following subsection. Both these edges originate at nodes which represent uncertain demand. Thus, these edges are expected to be extremely sensitive to changes in input and therefore qualify as good candidates for experimentation.

4.2 Results: Sparse Grid

Numerical results from all three analyses outlined in the foregoing section have been presented here, in a relatively similar order. The first is Figure 4.2, a plot of traffic volume flow frequencies for edges 26 and 32 - captured using kernel density estimation and probability-normalized histograms. The distribution of traffic volume on edge 32 resembles a symmetric bell-shape whereas the distribution of vehicles on edge 26 is positively skewed. However, the key takeaway here is that Smolyak sparse grid technique can recover output distributions as equally well as the more expensive Monte Carlo sampling approach. The red and blue histograms closely overlap creating a violet shade. Curves representing kernel density estimates are also well aligned with each other. This is true for both edges.

Additionally, variability of traffic volume on both edges has increased with increase in system uncertainty from 16 OD pairs to 64. Mode, the most frequent value, for both edges has remained same at approximately 2.5 and 3.5 for q_{26} and q_{32}, respectively. Tail length in q_{26} increased significantly from Figure 4.2a to Figure 4.2c but did not undergo much change afterwards. In fact, distributions in Figure 4.2c and Figure 4.2e are very similar in all regards. Same has happened in the case of q_{32} with significant increase in tail lengths from Figure 4.2b to Figure 4.2d and striking similarities between the latter and Figure 4.2f.

Table 4.1 and Figures 4.3 through 4.5 present errors encountered in estimating statistical moments of traffic volume flow on edges 26 and 32, once again comparing the Monte Carlo

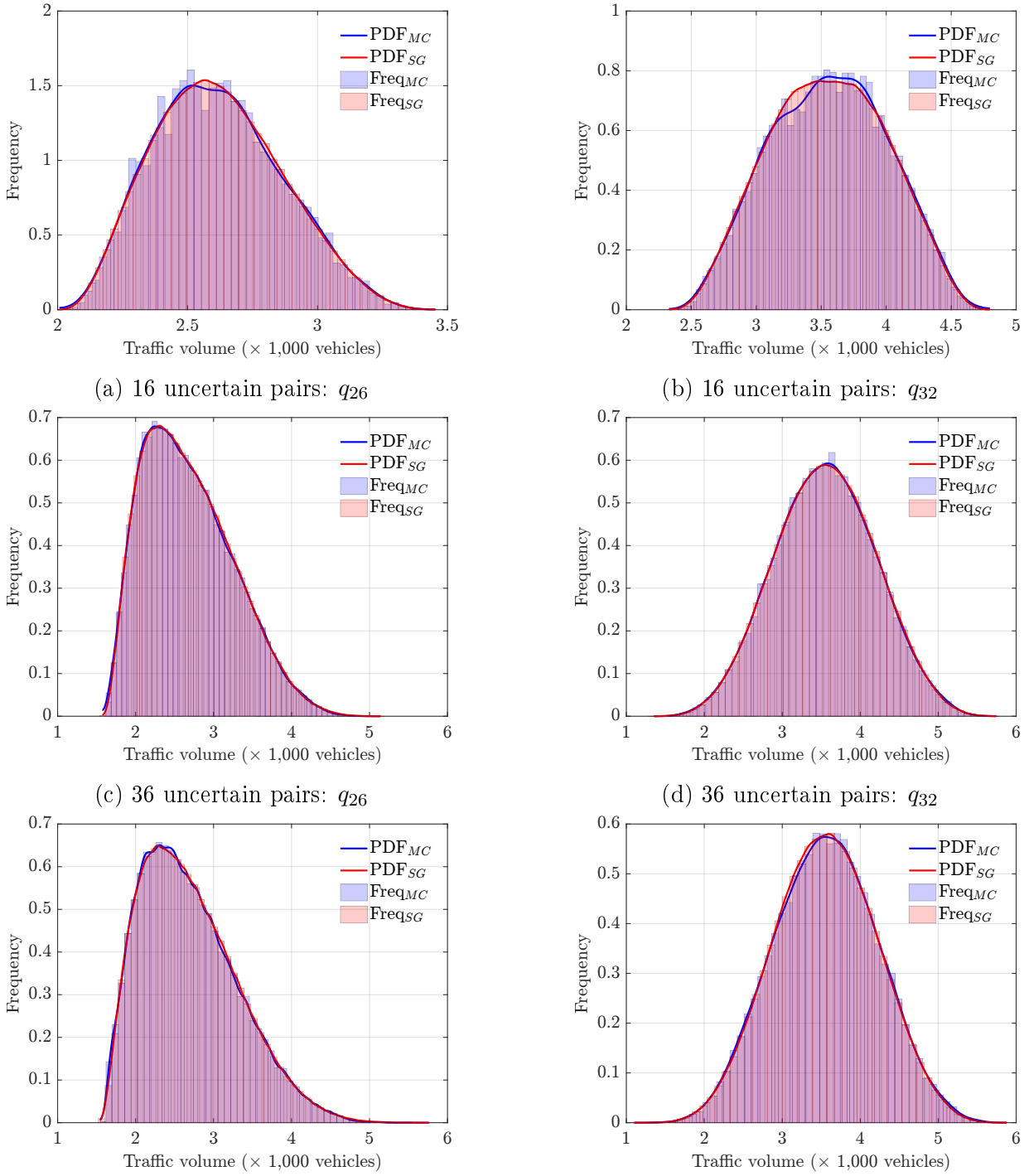

(a) 16 uncertain pairs: q_{26}

(b) 16 uncertain pairs: q_{32}

(c) 36 uncertain pairs: q_{26}

(d) 36 uncertain pairs: q_{32}

(e) 64 uncertain pairs: q_{26}

(f) 64 uncertain pairs: q_{32}

Figure 4.2: Kernel density estimates and accompanying histograms based on solution vectors $\{q_{mc}^{(i)}\}_{i=1}^{M_{mc}}$ and $\{q_{sg}^{(i)}\}_{i=1}^{M_t}$. All values in thousands of vehicles.

and sparse grid techniques. Here it should be noted that construction of a 64-dimensional level 2 interpolant, $\mathcal{A}_{2,64}$, required $M = 8,321$ points. It can be seen from Table 4.1 that

Monte Carlo sampling required 42,663 and 26,637 points for edges 26 and 32, respectively. This difference is captured in a relative sense by the time ratio which is roughly 5 and 3.3 for edges 26 and 32, respectively. Errors in mean estimates using Monte Carlo sampling technique were 11 vehicles for edge 26 and 3 vehicles in the case of edge 32. Both these values were higher than the sparse grid mean estimate errors of 5 vehicles in edge 26 and less than 1 vehicle in edge 32. Similar results were obtained for errors in standard deviation estimates with sparse grid performing at least as good as the Monte Carlo technique, using many times fewer samples. Lesser disparity was observed between the two techniques with both having an error of 1 vehicle in edge 26 and approximately 5 vehicles in edge 32.

Table 4.1: Errors in statistical estimates, comparison of Monte Carlo and Sparse Grid sampling, demonstrated for edges 26 and 32. All values in thousands of vehicles.

Edge	$\boldsymbol{\epsilon_{\bar{q},mc}}$	$\boldsymbol{\epsilon_{\bar{q},sg}}$	$\boldsymbol{\epsilon_{\sigma,mc}}$	$\boldsymbol{\epsilon_{\sigma,sg}}$	$\mathbf{M}_{mc}$	$\boldsymbol{\tau}$
26	0.011	0.005	0.001	0.001	42,663	4.867
32	0.003	< 0.001	0.005	0.004	26,637	3.316

Another notable feature of Figures 4.3 through 4.5 is that $\epsilon_{\bar{q},mc}$ and $\epsilon_{\sigma,mc}$ in all three levels of travel demand uncertainty are higher or equal to $\epsilon_{\bar{q},sg}$ and $\epsilon_{\sigma,sg}$ which is pictorially depicted by the orange dot representing Smolyak sparse grid estimate being positioned lower than the blue line representing Monte Carlo estimate. No general statements can be made comparing the gaps of $\epsilon_{\bar{q}}$ and ϵ_{σ} across the three uncertainty levels.

Figure 4.6 and Figure 4.7 depict the functional relationship between input uncertain travel demand and output traffic flow volumes, q_i, on edges under consideration when 16 OD pairs have been modeled uncertain. OD pairs originating from node 10 have been considered for edge 26 and those sharing node 11 as a common origin have been examined for edge 32. It can be seen that q_{26} depends linearly on $d_{10,2}$, somewhat linearly on $d_{10,3}$, and has a non-linear dependence on $d_{10,4}$ and $d_{10,8}$. q_{32} has a strictly linear relationship with all demands. The wide standard deviation margins should be noticed. The non-smoothness of response surface is another noteworthy observation.

Figures 4.8 and 4.9 explore the same functional relationship between traffic volumes on edges and travel demand values in case of 36 uncertain OD pairs. As a result, there are 6 subplots for each edge in this case. Same origin nodes as last case have been used - node 10 for q_{26} and node 11 for q_{32}. These specific nodes were chosen since edges 26 and 32 originate from nodes 10 and 11, respectively, and it is expected that q_{26} and q_{32} will be most sensitive to perturbations in travel demands originating here. Key features to note in this figure pair are:

1. q_{26} has non-linear dependence on the two newly added uncertain demand pairs - $d_{10,13}$

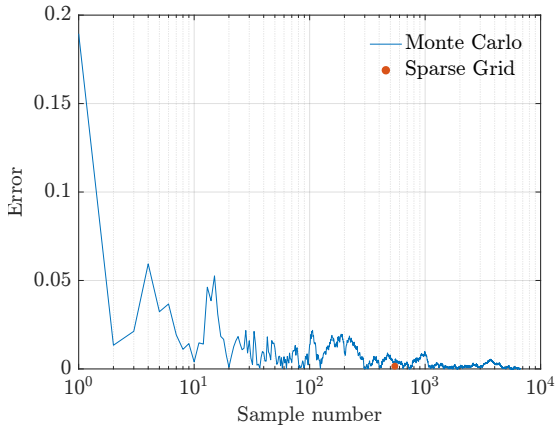

(a) $\epsilon_{\bar{q}}$, edge: 26

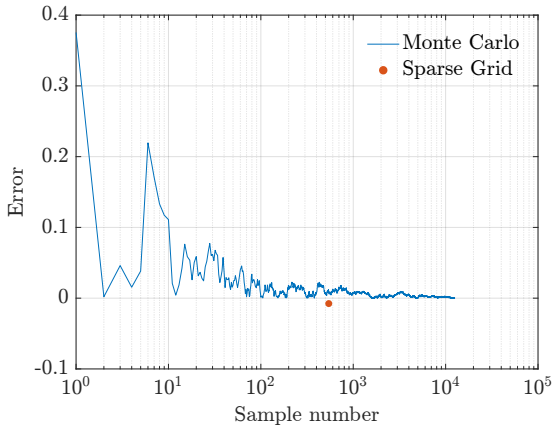

(b) $\epsilon_{\bar{q}}$, edge: 32

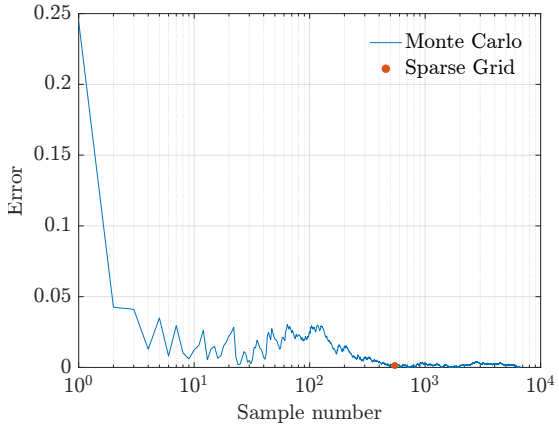

(c) ϵ_{σ}, edge: 26

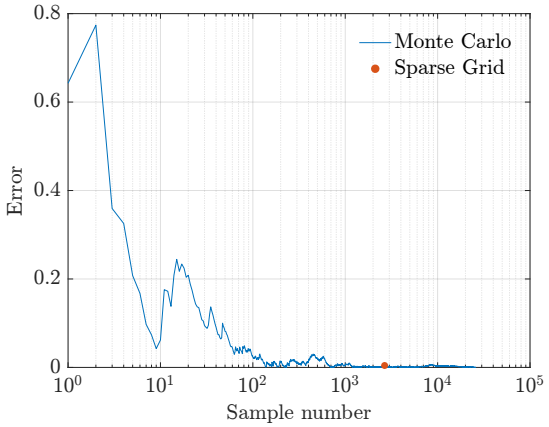

(d) ϵ_{σ}, edge: 32

Figure 4.3: 16 uncertain pairs - Errors in statistical estimates - mean(above) and standard deviation (below). $\epsilon_{\bar{q},mc}$ and $\epsilon_{\sigma,mc}$ plotted as blue lines, and $\epsilon_{\bar{q},sg}$ and $\epsilon_{\sigma,sg}$ marked with orange dots. All values in thousands of vehicles.

and $d_{10,15}$.

2. q_{32} is linearly related to the newly added demand pairs - $d_{11,13}$ and $d_{11,15}$.

Functional relationship under full extent of travel demand uncertainty - represented by 64 OD pairs - has been depicted in Figures 4.10 and 4.11. Once again, the same origins - nodes 10 and 11 have been considered while 2 additional destination locations have been added from the previous case of 36 OD pairs. Two key observations are - with increase in degree of uncertainty in the system, q_{26} has begun displaying non-linear dependence on most travel demands whereas q_{32} still demonstrates strict linear relationships with all uncertain demand pairs.

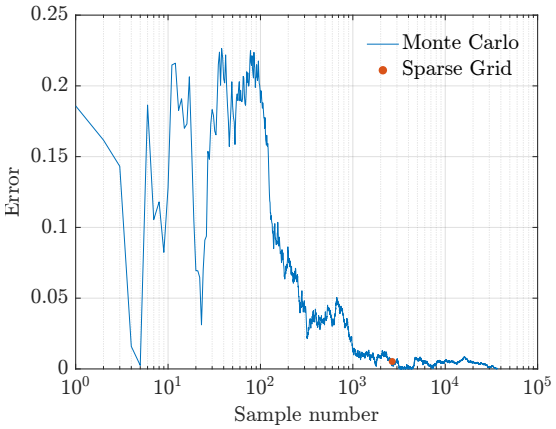

(a) $\epsilon_{\bar{q}}$, edge: 26

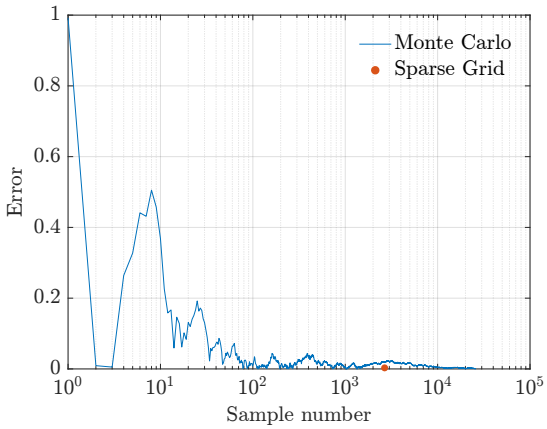

(b) $\epsilon_{\bar{q}}$, edge: 32

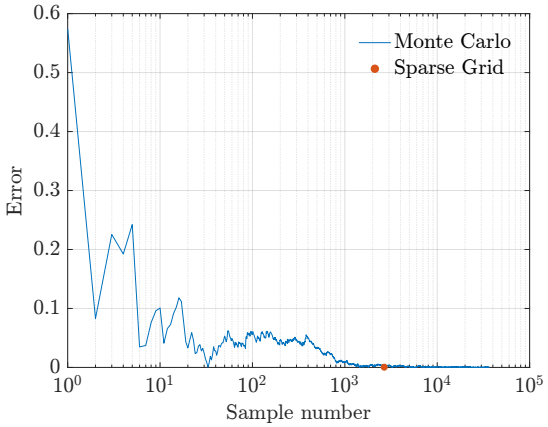

(c) ϵ_{σ}, edge: 26

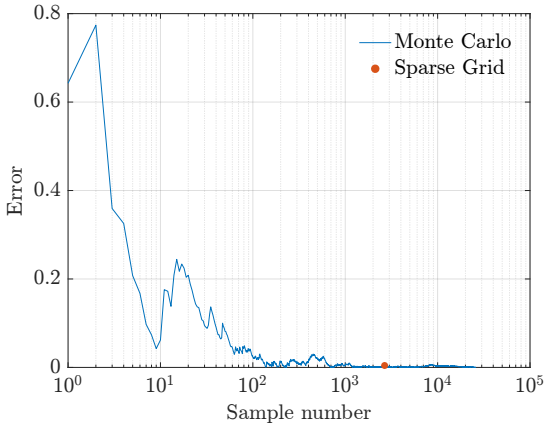

(d) ϵ_{σ}, edge: 32

Figure 4.4: 36 uncertain pairs - Errors in statistical estimates - mean(above) and standard deviation (below). $\epsilon_{\bar{q},mc}$ and $\epsilon_{\sigma,mc}$ plotted as blue lines, and $\epsilon_{\bar{q},sg}$ and $\epsilon_{\sigma,sg}$ marked with orange dots. All values in thousands of vehicles.

4.3 Results: PCE

User equilibrium problems were solved 500,000 times for the entire network using 64-dimensional realization sets. Second-order PCE surrogates were then constructed using these samples for all the 76 edges. Most surrogates were found to have linear dependence on the input, however a few edges showed non-linearity. One of these edges is edge 26 connecting nodes 10 and 9. It should be noted that node 10 belongs to $O_{uncertain}$. The PCE coefficients so obtained are considered ground truth.

A second-order 64-dimensional PCE results in 2,145 basis functions, each associated to a coefficient in the expansion, see equation 2.26. Figure 4.12 shows coefficients amplitudes for all 2,145 coefficients. These have been obtained using the least-squares method after creating the measurement matrix. Further, 10^{-2} has been considered the cutoff threshold of impor-

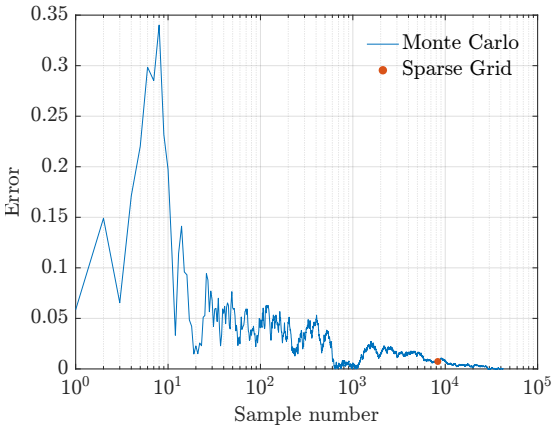

(a) $\epsilon_{\bar{q}}$, edge: 26

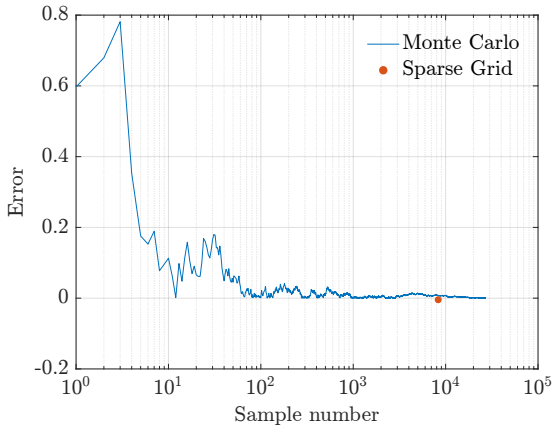

(b) $\epsilon_{\bar{q}}$, edge: 32

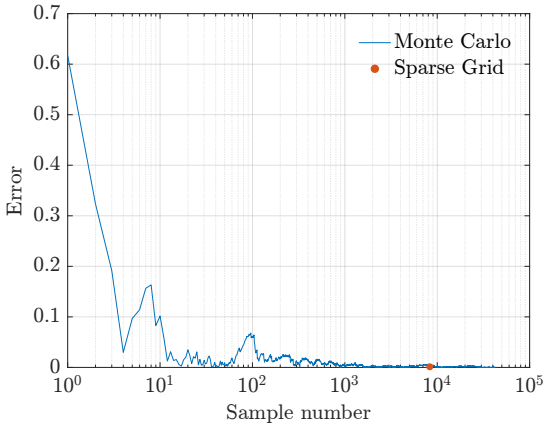

(c) ϵ_{σ}, edge: 26

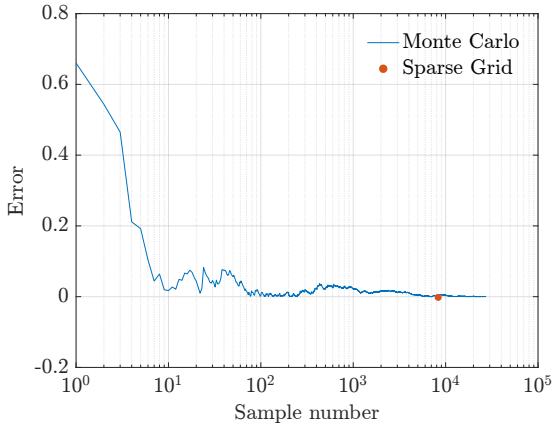

(d) ϵ_{σ}, edge: 32

Figure 4.5: 64 uncertain pairs - Errors in statistical estimates - mean(above) and standard deviation (below). $\epsilon_{\bar{q},mc}$ and $\epsilon_{\sigma,mc}$ plotted as blue lines, and $\epsilon_{\bar{q},sg}$ and $\epsilon_{\sigma,sg}$ marked with orange dots. All values in thousands of vehicles.

tance to identify influential coefficients and the dimensions represented by these are also plotted. The importance of a dimension depends on 2 factors - 1. the number of coefficients it affects, and 2. the amplitudes of these corresponding coefficients, with higher amplitudes representing higher importance. Based on these criteria, from Figure 4.12, it can be concluded that dimension 42 is the most important since it corresponds to a high concentration of high amplitude coefficients. Following are dimensions 58 and 34 which also represent high concentrations. It is interesting to note that most of the uncertainty in a 64-dimensional problem can be explained by 13 dimensions viz. $\{2, 10, 17, 18, 25, 26, 33, 34, 41, 42, 50, 57, 58\}$.

Table 4.2 provides detailed information on the important dimensions identified by each surrogate along with its order, statistical values estimated using the surrogate, and its cross-validation performance in terms of L2-error. The dimension reduction algorithm performed consistently well and captured dimensions $\{42, 34, 58, 26, 18, 50, 2, 10\}$ for all sample sets

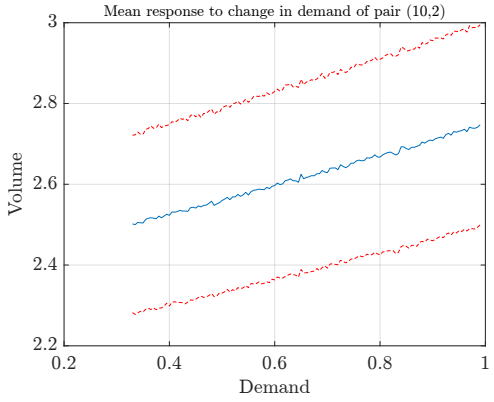

(a) q_{26} vs. $d_{10,2}$

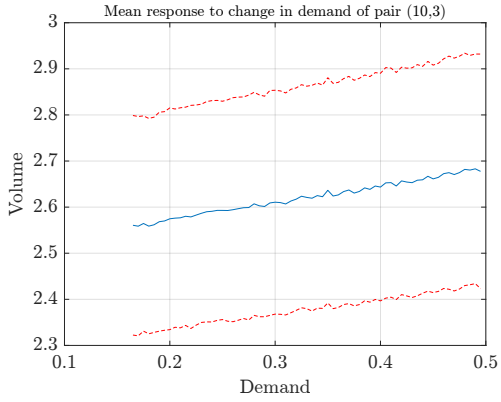

(b) q_{26} vs. $d_{10,3}$

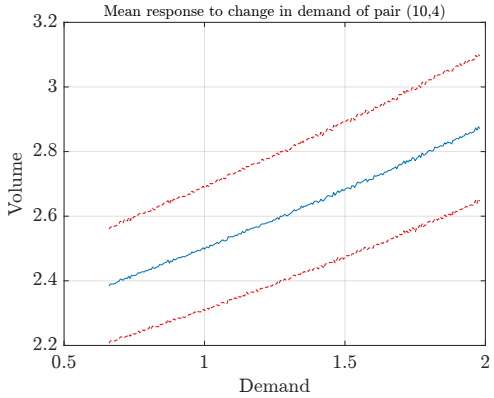

(c) q_{26} vs. $d_{10,4}$

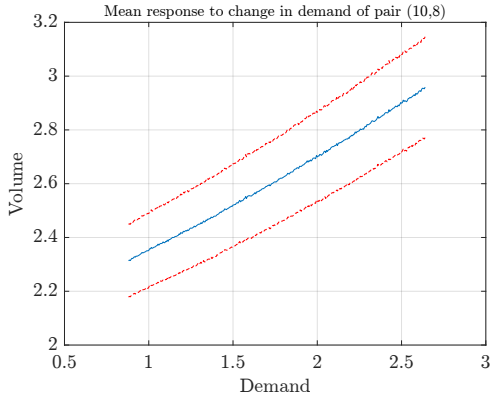

(d) q_{26} vs. $d_{10,8}$

Figure 4.6: 16 uncertain pairs - Functional relationship of output traffic flow volume on edge 26 with uncertain travel demand. Mean and mean $\pm$ 1 standard deviation plotted. All values in thousands of vehicles.

of size 300 and 500. Even the sets of size 100 were able to capture the 4 most important dimensions $\{42, 34, 58, 26\}$ at all locations and for both error thresholds. Surrogates obtained using error threshold 10^{-2} were of order 3 for sample size 100 and of order 2 and dimension 9 for larger sample sets with the first 8 dimensions being the important ones and ninth varying depending on sampling location. In the case of error threshold 10^{-3}, surrogates for sample sizes 100 and 300 were a mix of orders 3 and 4 while all surrogates for sample size 500 were of order 4. Dimensionality of the surrogates for sizes 300 and 500 was strictly 8 in this case.

Figures 4.13 and 4.14 show the cross-validation performance of the reduced dimension PCE surrogates. A testing sample set of size 100 was used for this purpose. Four key

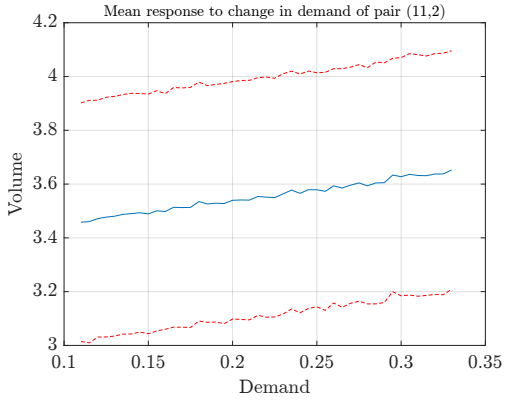

(a) q_{32} vs. $d_{11,2}$

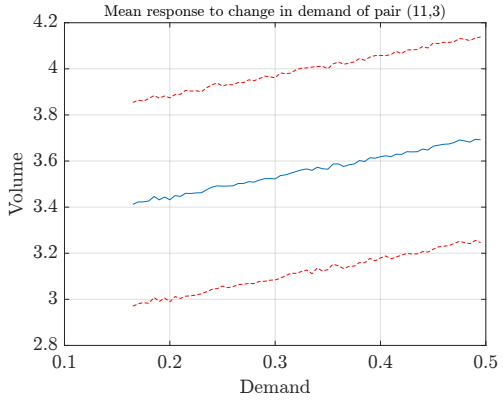

(b) q_{32} vs. $d_{11,3}$

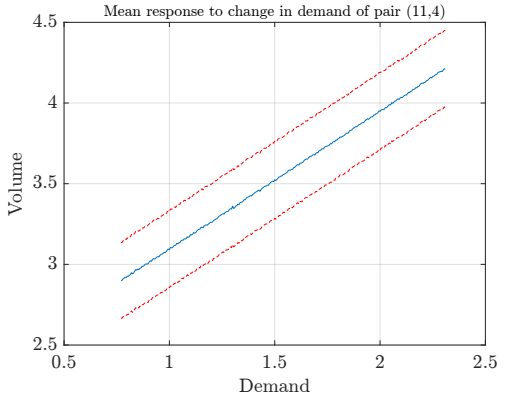

(c) q_{32} vs. $d_{11,4}$

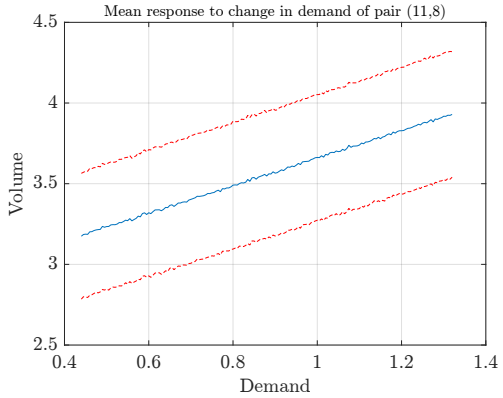

(d) q_{32} vs. $d_{11,8}$

Figure 4.7: 16 uncertain pairs - Functional relationship of output traffic flow volume on edge 32 with uncertain travel demand. Mean and mean $\pm$ 1 standard deviation plotted. All values in thousands of vehicles.

conclusions can be drawn from the plot:

1. Surrogates based on sample sizes 300 and 500 perform better than ones based on 100 samples - this is due to the fact that while the 100 sample surrogate captures 4 most important dimensions, it also excludes 4 lesser important dimensions.
2. Performance of the surrogate obtained using error threshold 10^{-2} (Figure **??**) is better than the one obtained using 10^{-3} threshold - this may be due to the additional dimension captured in the 10^{-2} case. This indicates a higher influence of dimensions on surrogate quality as compared to order.
3. Sample sizes 300 and 500 have very similar performance with 300 performing slightly

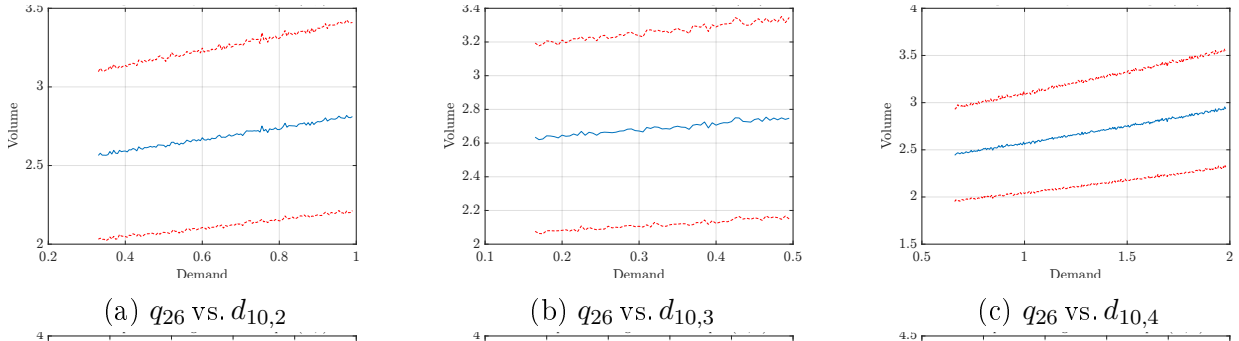

(a) q_{26} vs. $d_{10,2}$ (b) q_{26} vs. $d_{10,3}$ (c) q_{26} vs. $d_{10,4}$

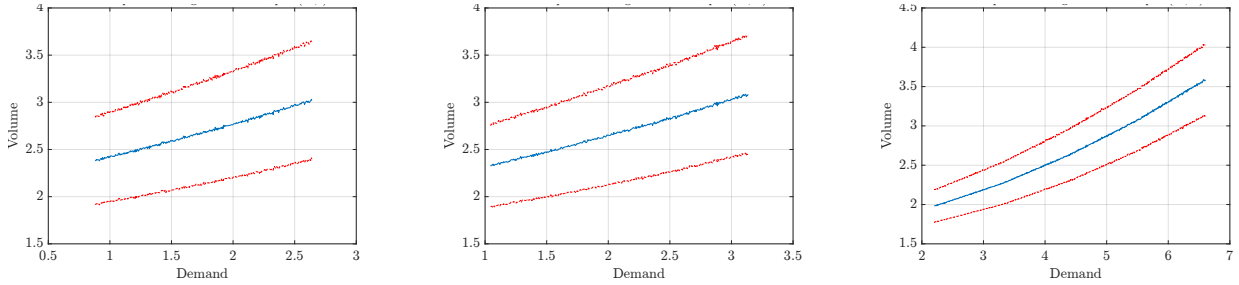

(d) q_{26} vs. $d_{10,8}$ (e) q_{26} vs. $d_{10,13}$ (f) q_{26} vs. $d_{10,15}$

Figure 4.8: 36 uncertain pairs - Functional relationship of output traffic flow volume on edge 26 with uncertain travel demand. Mean and mean ± 1 standard deviation plotted. All values in thousands of vehicles.

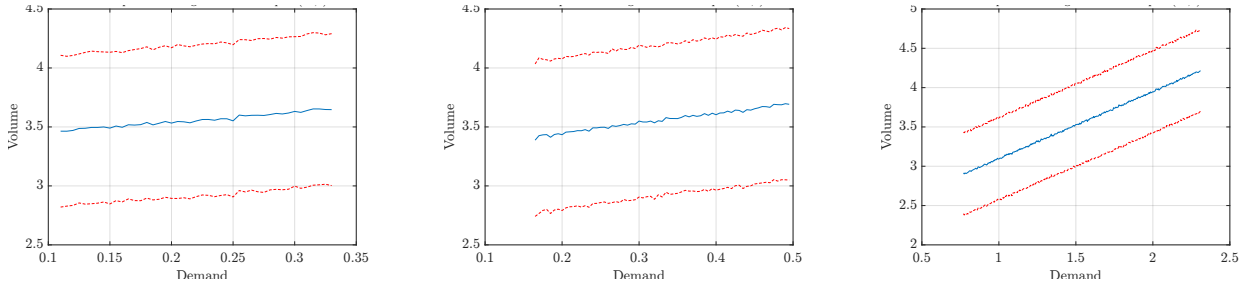

(a) q_{32} vs. $d_{11,2}$ (b) q_{32} vs. $d_{11,3}$ (c) q_{32} vs. $d_{11,4}$

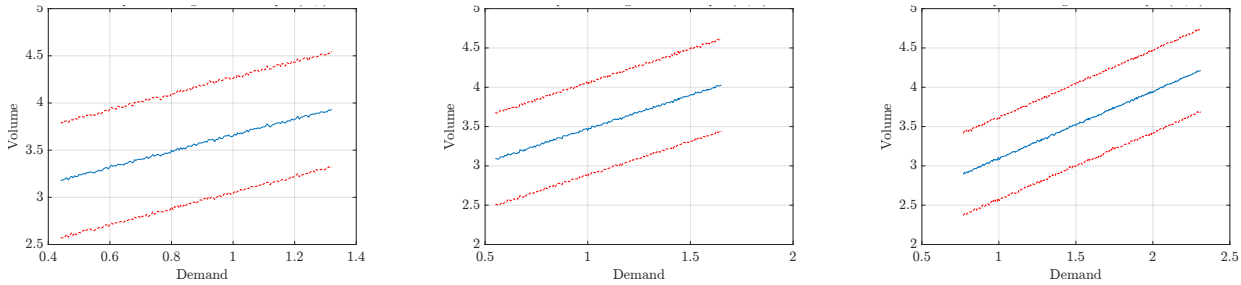

(d) q_{32} vs. $d_{11,8}$ (e) q_{32} vs. $d_{11,13}$ (f) q_{32} vs. $d_{11,15}$

Figure 4.9: 36 uncertain pairs - Functional relationship of output traffic flow volume on edge 32 with uncertain travel demand. Mean and mean ± 1 standard deviation plotted. All values in thousands of vehicles.

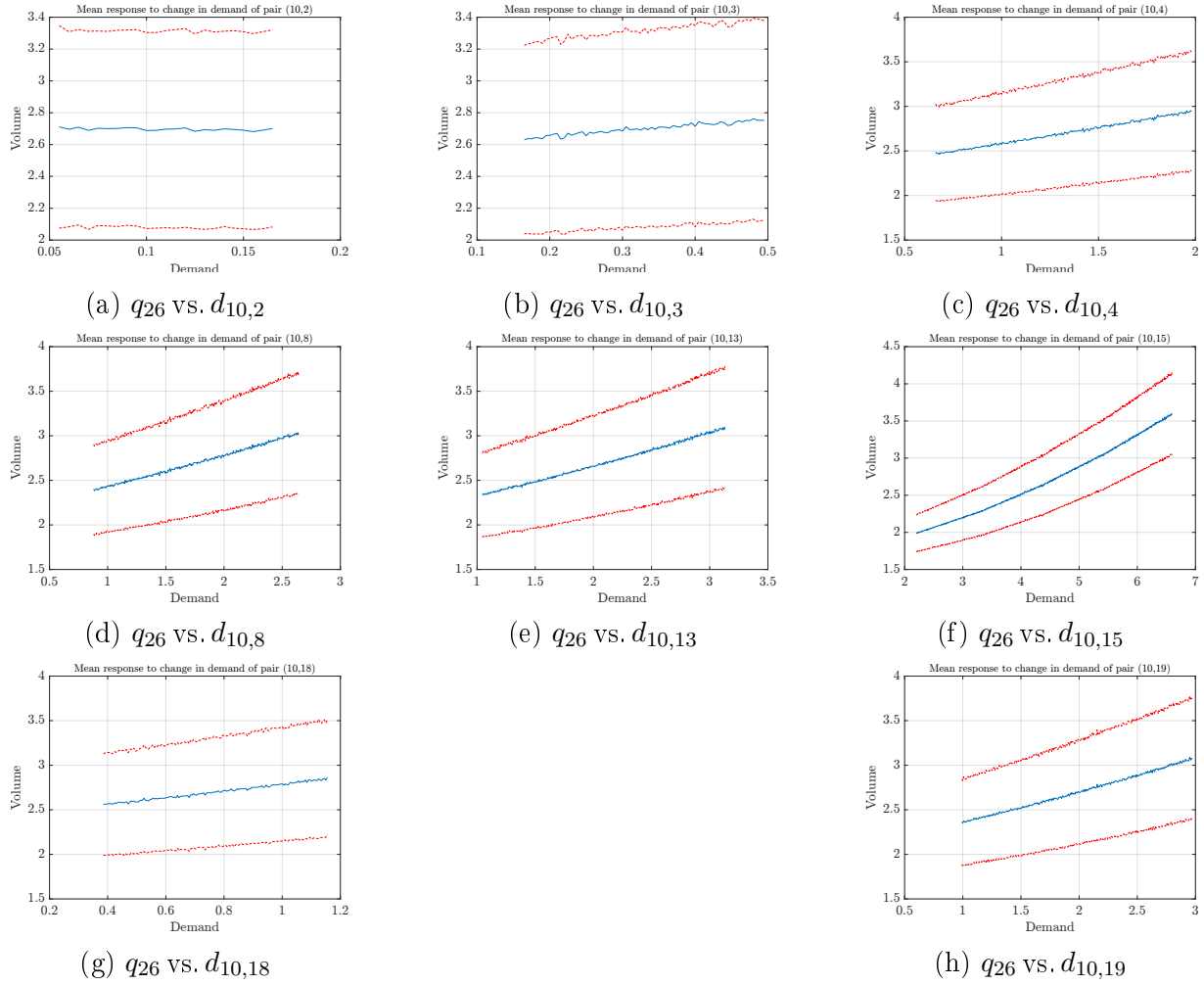

(a) q_{26} vs. $d_{10,2}$ (b) q_{26} vs. $d_{10,3}$ (c) q_{26} vs. $d_{10,4}$

(d) q_{26} vs. $d_{10,8}$ (e) q_{26} vs. $d_{10,13}$ (f) q_{26} vs. $d_{10,15}$

(g) q_{26} vs. $d_{10,18}$ (h) q_{26} vs. $d_{10,19}$

Figure 4.10: 64 uncertain pairs - Functional relationship of output traffic flow volume on edge 26 with uncertain travel demand. Mean and mean $\pm$ 1 standard deviation plotted. All values in thousands of vehicles.

better in the 10^{-3} case.

4. Performance has little dependence on sampling location for training data - all 5 sets within Figures 4.13 and 4.14 appear relatively similar.

Histograms that serve as further proofs of cross-validation have been presented in Appendix B. They are an alternative representation form of the information presented in the diagonal plots.

A surrogate constructed using 300 samples and error threshold 10^{-2} was found to have an L2-norm value of 0.0298, much lower than the surrogate using 100 samples which resulted in 2.0660. The lowest value of 0.0287 was obtained using 500 samples which is a marginal improvement considering the increase in number of samples. All surrogates constructed with

Table 4.2: Important dimensions, order, mean and variance, and cross validation L2-error term ϵ for surrogates constructed using greedy algorithm for dimension reduction.

Size	**Error**	10^{-2}					10^{-3}				
	Set	**Important dimensions**	**Order**	**Mean**	**Var**	ϵ	**Important dimensions**	**Order**	**Mean**	**Var**	ϵ
500	1	$\{42, 34, 58, 26, 18, 50, 2, 10, 6\}$	2	2.6941	0.3849	0.0278	$\{42, 34, 58, 26, 18, 50, 2, 10\}$	4	2.6940	0.3913	0.7002
	2	$\{42, 58, 34, 26, 18, 50, 2, 10, 4, 28\}$	2	2.6950	0.3855	0.0279	$\{42, 58, 34, 26, 18, 50, 2, 10\}$	4	2.7013	0.3883	0.3316
	3	$\{42, 58, 34, 26, 18, 50, 2, 10, 28, 15\}$	2	2.6939	0.3847	0.0287	$\{42, 58, 34, 26, 18, 50, 2, 10\}$	4	2.6948	0.4073	0.4756
	4	$\{42, 34, 58, 26, 18, 50, 2, 10, 6\}$	2	2.6938	0.3853	0.0273	$\{42, 34, 58, 26, 18, 50, 2, 10\}$	4	2.6913	0.3931	0.3273
	5	$\{42, 58, 34, 26, 18, 50, 2, 10, 35\}$	2	2.6945	0.3853	0.0274	$\{42, 58, 34, 26, 18, 50, 2, 10\}$	4	2.6889	0.4021	0.4238
300	1	$\{42, 34, 58, 26, 18, 50, 2, 10, 28\}$	2	2.6948	0.3853	0.0277	$\{42, 34, 58, 26, 18, 50, 2, 10, 8\}$	4	2.6980	0.3977	0.4745
	2	$\{42, 58, 34, 26, 18, 50, 2, 10, 4, 36, 12\}$	2	2.6949	0.3857	0.0285	$\{42, 58, 34, 26, 18, 50, 2, 10, 1\}$	4	2.7000	0.3900	0.2991
	3	$\{42, 34, 58, 26, 18, 50, 2, 10, 6\}$	2	2.6937	0.3847	0.0298	$\{42, 34, 58, 26, 18, 50, 2, 10, 7\}$	3	2.6946	0.3863	0.0507
	4	$\{42, 58, 34, 26, 18, 50, 2, 10, 5\}$	2	2.6935	0.3858	0.0300	$\{42, 34, 58, 26, 18, 50, 2, 10, 9\}$	3	2.6952	0.3963	0.0568
	5	$\{42, 58, 34, 26, 18, 50, 2, 10, 36\}$	2	2.6944	0.3855	0.0284	$\{42, 58, 34, 26, 18, 50, 2, 10, 28\}$	3	2.6936	0.3859	0.0461
100	1	$\{42, 34, 58, 26, 18, 23\}$	3	2.7448	0.5601	1.1197	$\{42, 34, 58, 26, 18\}$	4	2.7835	1.7720	3.9445
	2	$\{42, 34, 58, 26, 18, 50\}$	3	2.6941	0.5438	1.7138	$\{42, 34, 58, 26, 18, 50, 1\}$	3	2.6212	0.5955	1.3672
	3	$\{42, 34, 58, 26, 18, 50, 7\}$	3	2.7805	0.6520	2.0660	$\{42, 34, 58, 26, 18, 50, 1\}$	3	2.8278	1.2244	3.1969
	4	$\{42, 34, 58, 26, 18, 50\}$	3	2.6498	0.4720	1.1525	$\{42, 34, 58, 26, 18, 50, 1\}$	3	2.8035	0.7085	2.1235
	5	$\{42, 58, 34, 26, 18, 27\}$	3	2.6429	0.4871	1.7960	$\{42, 58, 34, 26, 18\}$	4	2.7358	1.0715	4.2842

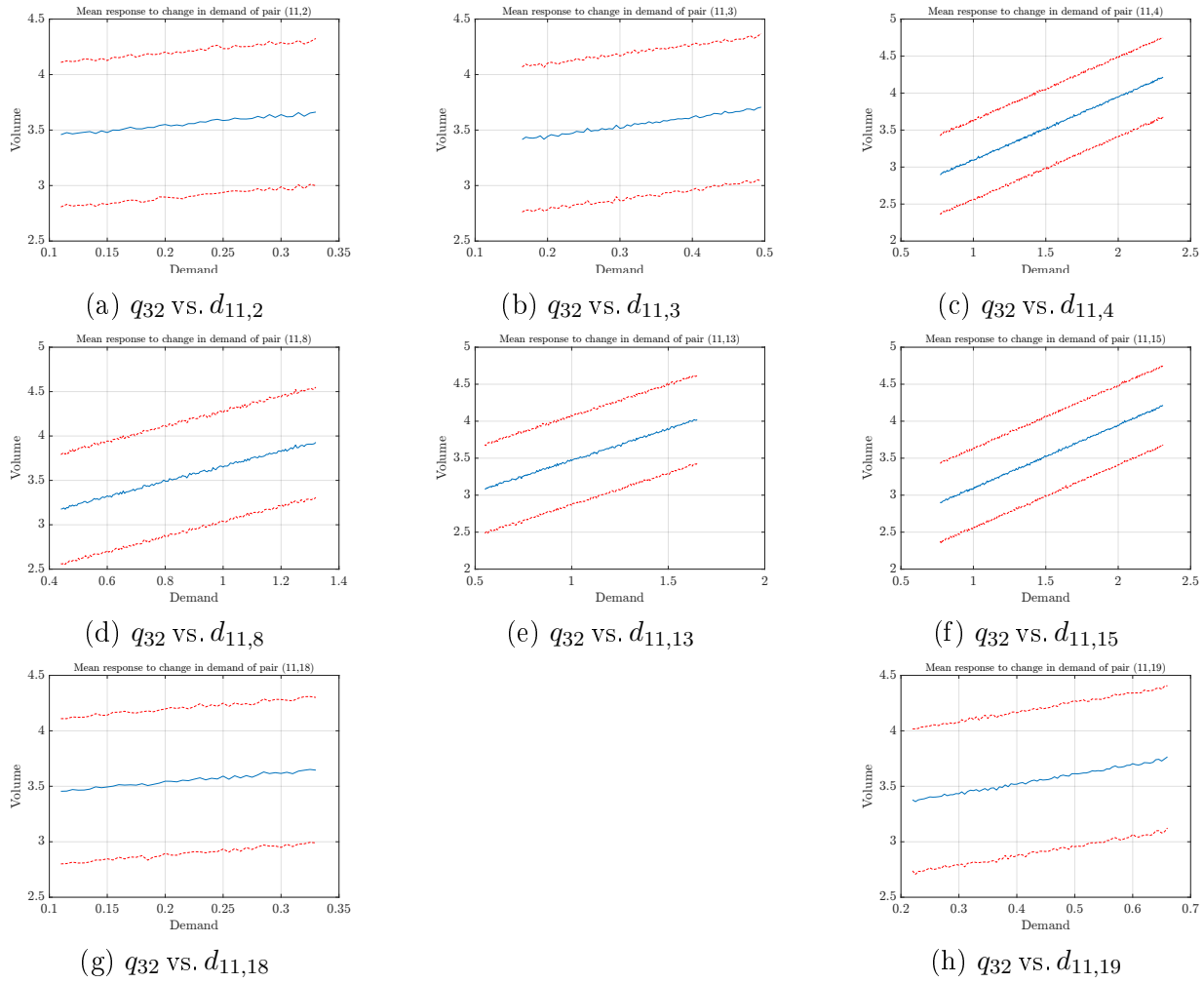

(a) q_{32} vs. $d_{11,2}$ (b) q_{32} vs. $d_{11,3}$ (c) q_{32} vs. $d_{11,4}$

(d) q_{32} vs. $d_{11,8}$ (e) q_{32} vs. $d_{11,13}$ (f) q_{32} vs. $d_{11,15}$

(g) q_{32} vs. $d_{11,18}$ (h) q_{32} vs. $d_{11,19}$

Figure 4.11: 64 uncertain pairs - Functional relationship of output traffic flow volume on edge 32 with uncertain travel demand. Mean and mean $\pm$ 1 standard deviation plotted. All values in thousands of vehicles.

error threshold 10^{-2} performed better than their 10^{-3} counterparts.

Consequently, the 300 sample 10^{-2} error threshold surrogate has been used for all further analyses. A concrete proof of performance is presented in Figure 4.15, where estimated traffic volumes have been cross-validated against true values for 500,000 samples. Volumes less than 5 align perfectly with true data, but the surrogate tends to slightly overestimate higher volumes resulting in deviation from the $y = x$ line. Table 4.3 offers statistical comparison between the surrogate estimates and true values. Mean value of 2.6937 is estimated which is accurate up to 2 decimal places as compared to the true value 2.6943. Difference between the two values is 0.0006. The variance estimates differs from true value by only 0.0002. Since traffic volumes are represented in terms of vehicle numbers in thousand, both these differences represent an error of maximum 1 vehicle on an edge catering to over 2,600 vehicles.

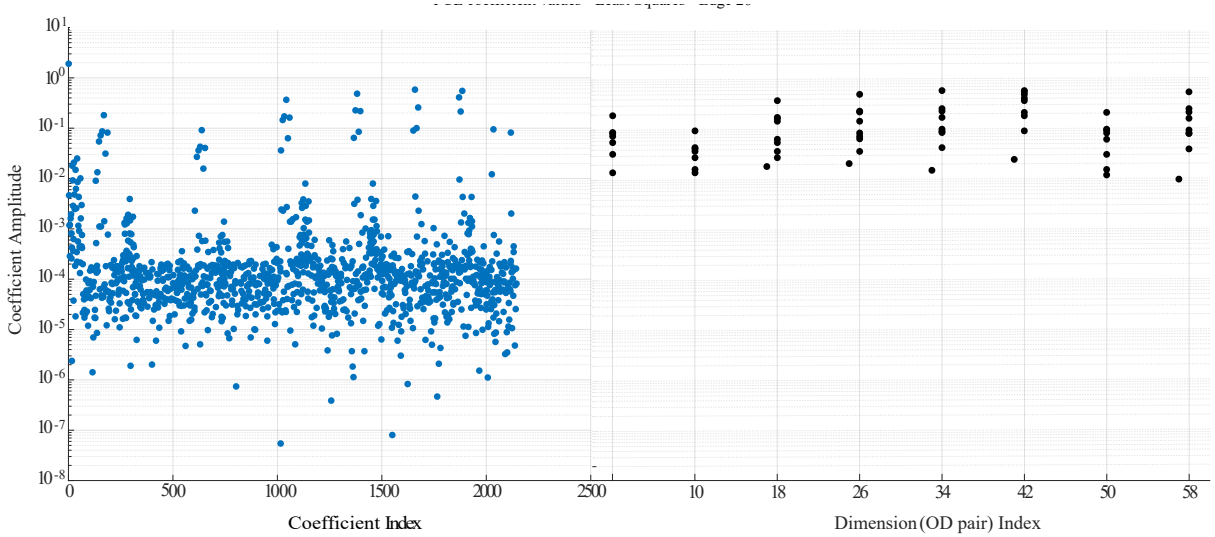

Figure 4.12: Coefficient amplitudes and dimensions corresponding to important coefficients for edge 26.

Table 4.3: Comparison of statistical values.

Statistic	**True Model**	**Surrogate**
Mean	2.6943	2.6937
Variance	0.3849	0.3847
Median	2.6040	2.6076

Further comparison is presented in Figure 4.16 which compares the median, quantiles and ranges via a box and whisker plot. Outliers have been marked using red crosses, the existence of which is a result of pure statistical treatment of data. Technically, the numbers represent vehicle volumes under varying demand conditions and there are no outliers as such. As it can be referred from the figure, all statistical values between the surrogate and true model have close to exact correspondence. The only discernible difference between the two is in terms of higher values represented as top few crosses, as previously discussed.

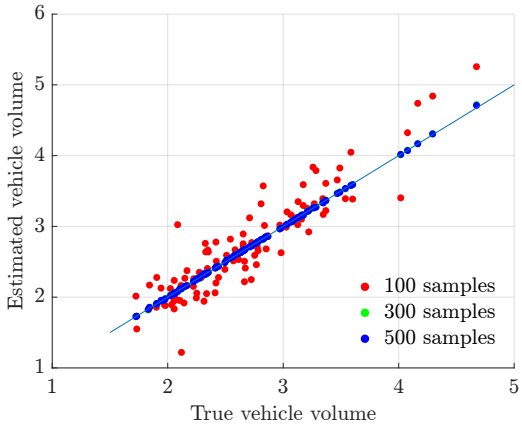

(a) Set 1

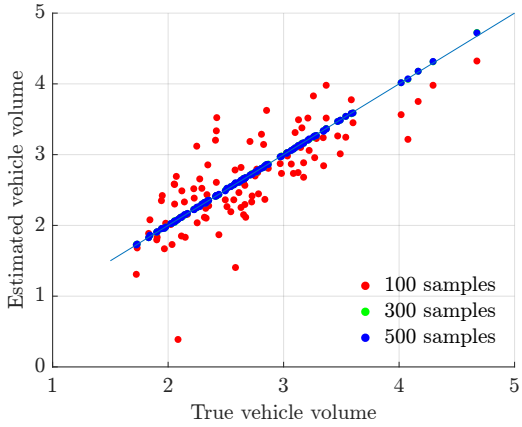

(b) Set 2

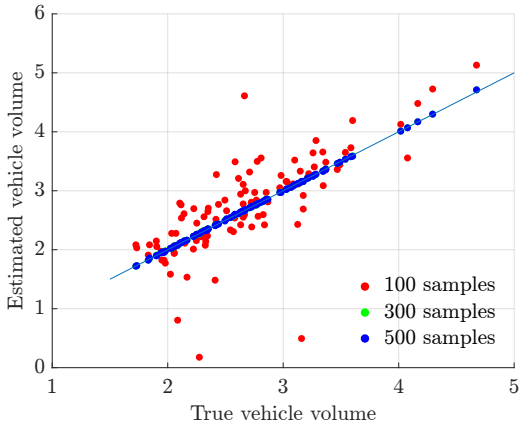

(c) Set 3

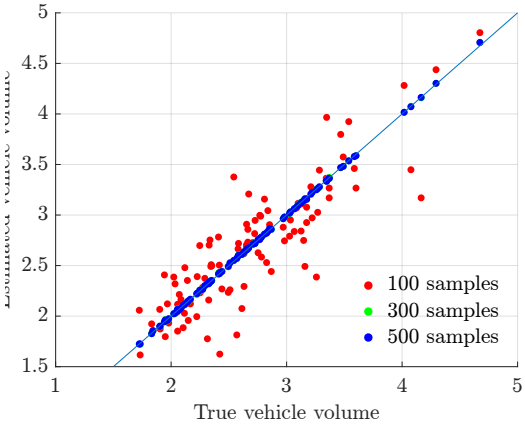

(d) Set 4

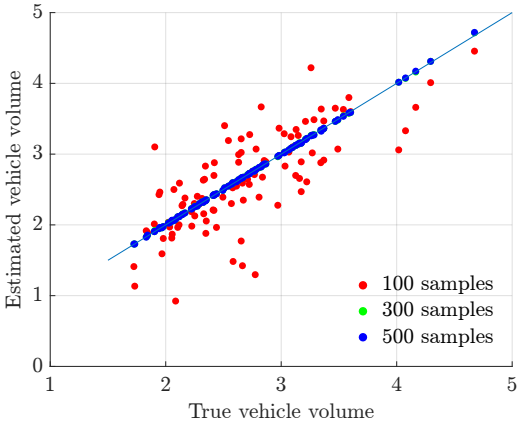

(e) Set 5

Figure 4.13: Cross-validation plots comparing true vehicle volumes with estimated volumes obtained using reduced dimension PCE surrogates with error threshold 10^{-2} and 5 different sampling locations for training data.

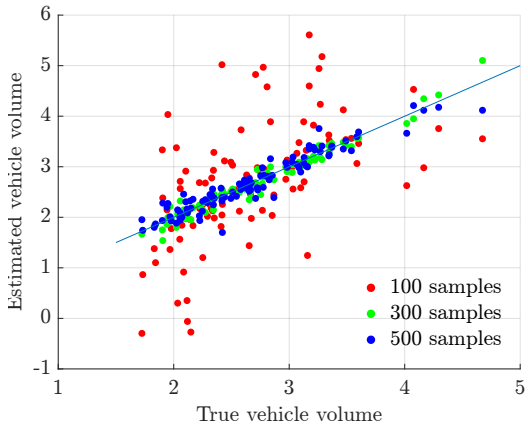

(a) Set 1

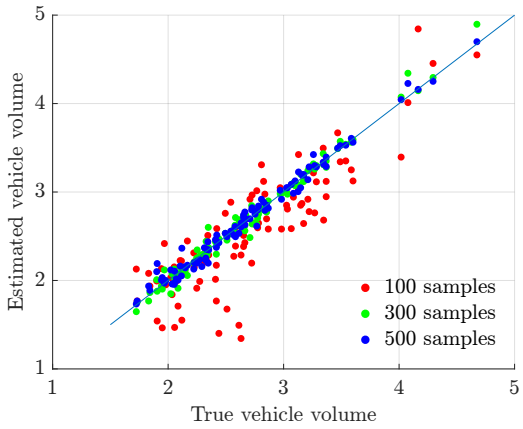

(b) Set 2

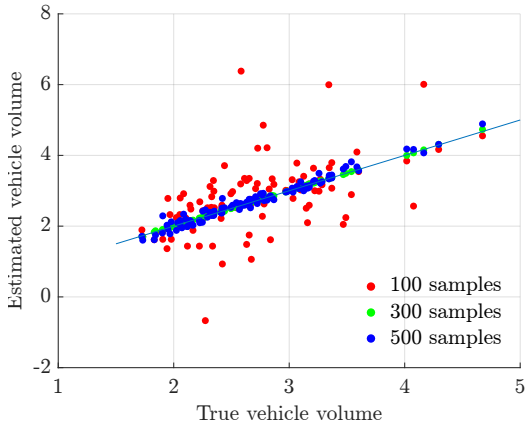

(c) Set 3

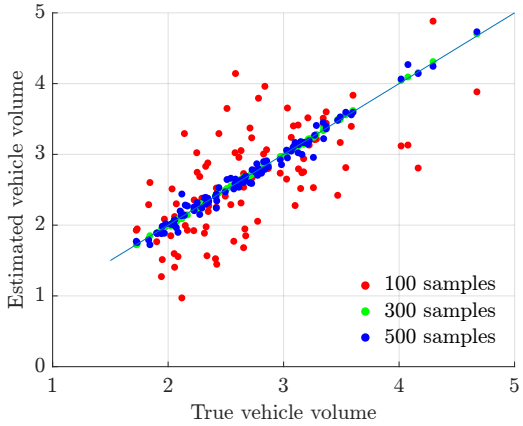

(d) Set 4

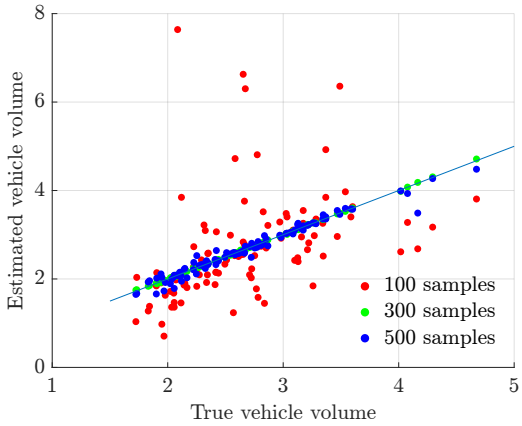

(e) Set 5

Figure 4.14: Cross-validation plots comparing true vehicle volumes with estimated volumes obtained using reduced dimension PCE surrogates with error threshold 10^{-3} and 5 different sampling locations for training data.

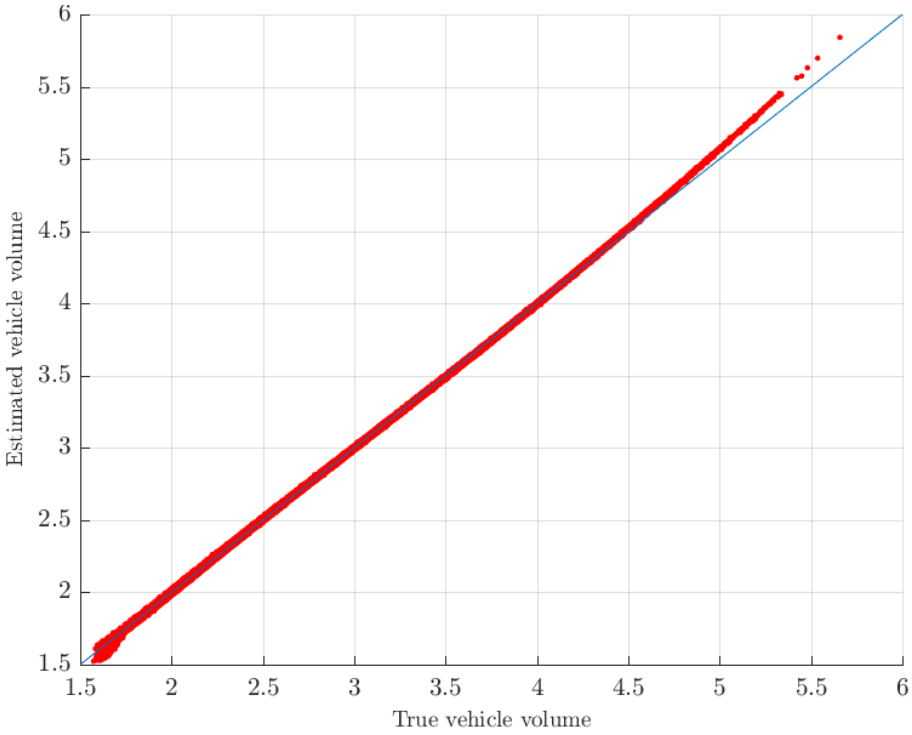

Figure 4.15: Cross-validation comparing true vehicle volume with estimate volume using 500,000 realization sets.

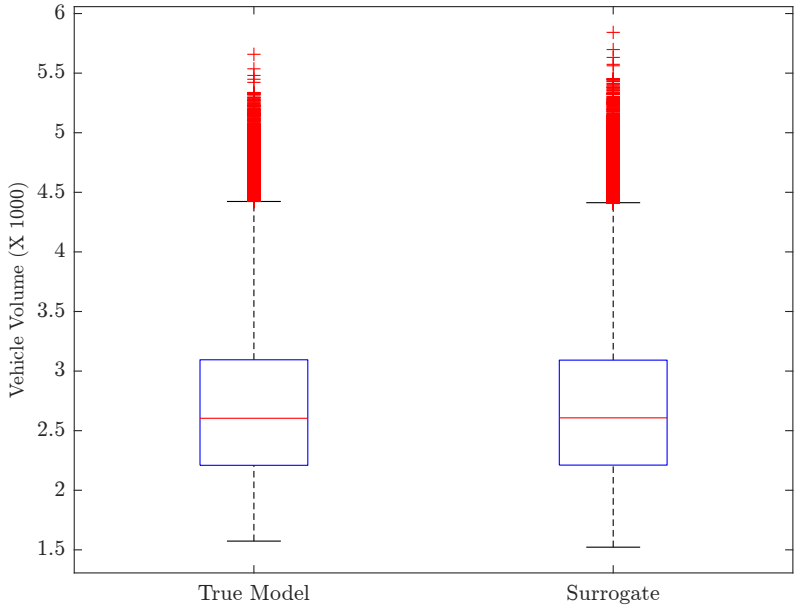

Figure 4.16: Comparison of median, quantiles and range. Outliers depicted as red crosses.

Chapter 5

Discussion

5.1 Sparse Grid

As mentioned previously, Figure 4.2 presents the most concrete proof of Smolyak sparse grid's performance. For both edges, complete distributions of traffic volume were constructed. Based on visual inspection of the histogram and kernel density estimates, it can safely be concluded that sparse grid performance closely matches that of Monte Carlo sampling. The distributions themselves are both bell-shaped curves with bulk of the occurrences concentrated in the 'head' of the curves. Tails in both cases are short with few occurrences present away from the central values. This is expected because the network user equilibrium trip assignment method has the tendency to produce stable and robust outputs even with uncertain inputs. Although no definite reasons are known for this phenomenon, it is hypothesized that traffic can be diverted and distributed on entirely new routes so as to avoid high costs on existing route options. It can be deduced from equation 4.1 that edge travel cost depends on traffic volume as per the *power law* defined in statistics. Therefore, while traffic assignment algorithm may choose the obvious low-cost option for moderate traffic volume, it may be beneficial to distribute high travel demand along multiple routes instead of channeling a high volume of vehicles along the prior low-cost option. This is because user equilibrium is a network-level optimization. Consequently, the traffic flow on any particular edge remains fairly constrained with large number of repeated occurrences around central values and few extreme observations.

Figures 4.3 through 4.5 present a direct comparison between Monte Carlo sampling and Smolyak sparse grid approaches. These are plots of mean estimation error terms $\epsilon_{\bar{q},mc}$ and $\epsilon_{\bar{q},sg}$ defined in equations 3.2 and 3.4. As previously established, values at Monte Carlo convergence have been accepted as ground truth and sparse grid estimates have been compared against them. However, in order to ensure fair comparison, performance of Monte

Carlo at the number of samples required to construct the sparse grid interpolant has been considered. In most cases, it can visually be observed that error in the sparse grid estimate, represented by orange dot, is lower than Monte Carlo error at the same stage. The same isn't immediately clear in Figure 4.4a, but even in this case the error in sparse grid estimate is, in fact, lower. For the final test case scenario of 64 uncertain OD pairs, values have also been tabulated in Table 4.1. These have been used to facilitate following discussion. Since the error is less than 1 vehicle, the practical unit, it can be said that sparse grid technique *exactly* estimated the true mean. Smolyak grid is expected to have better performance than Monte Carlo given the same number of sampling points since these points are strategically located throughout the support to capture near complete information as opposed to random selection in the case of Monte Carlo. It should, however, be noted that in cases of low sensitivity of output to input, Monte Carlo sampling may converge with very few points while Smolyak sparse grid will still require the predetermined number of evaluations. Many such cases can be found in Appendix A. However, it should also be noted that only a subset of edges form paths between uncertain OD pairs and a smaller subset are lucrative inexpensive edges that form an essential part of these paths. Edges 26 and 32 both are examples of such edges and their sensitivity to change in travel demand has been exhibited in Figure 4.2.

Similar results have been observed in case of ϵ_σ sub-figures, plots of standard deviation estimation error terms $\epsilon_{\sigma,mc}$ and $\epsilon_{\sigma,sg}$ defined in equations 3.3 and 3.5. Again for edge 26, it can be concluded based on visual inspection that sparse grid performance is better than Monte Carlo at the same stage while edge 32 isn't immediately clear. Table 4.1 can be referred to for exact values, which confirm the conclusion made in the foregoing statement. It is interesting to note that the sparse grid approach is capable of producing comparable results using as many as 5 times lesser samples. These savings directly translate to computational effort reduction, which is a major concern in solving traffic assignment problems for large networks. All errors are in order of tens of vehicles on edges that typically carry volumes in thousands.

In all cases of Figures 4.3 through 4.5, it is interesting to note that Monte Carlo analysis reaches extremely low errors, less than sparse grid, during the early stages with less than 100 sample points. Technically in terms of deterministic code evaluations, it outperforms the Smolyak sparse grid approach by an order of magnitude if it were possible to terminate the algorithm at this early stage. However, this is not a possibility. Once a convergence criterion is set, the algorithm can only conclude once it is satisfied. Early convergence can be obtained by relaxing the criterion, but the estimates will then suffer from loss of accuracy. This work is an effort to produce accurate estimates of traffic volume under demand uncertainty and setting large convergence tolerances will defeat the primary purpose. Following a

three step approach of increasing uncertainty has helped demonstrate performance in both medium and high dimensional cases. Smolyak sparse grid outperforms Monte Carlo till up to 64 dimensions. Also, even in lower dimensional cases where Monte Carlo attains quick convergence, Sparse Grid still performs better on sensitive edges such as those considered in this study.

Figures 4.6 through 4.11 plot the functional relationship between traffic volumes q_i and travel demands $d_{k,l}$. For this analysis, the origin nodes k were selected such that they are also the originating nodes for edges being considered. Therefore, $k = 10$ for $i = 26$ and $k = 11$ for $i = 32$. Based on visual observation of the plots, edge 32 has linear dependence on all travel demands considered here. This represents a linearly proportional increase in traffic routed via a *cheap* edge with increase in travel demand originating from a node the edge is directly emergent from. It should also be noted that the spread of these travel demands is not too wide. Relationships observed in cases of 16 and 36 uncertain OD pairs are also observed in the final case of 64 pairs and so Figures 4.10 and 4.11 have been referred for the following discussion. Maximum variation is observed in $d_{11,4}$ and $d_{11,15}$ of 1,800 vehicles. Variations in all other cases are comparatively lower at less than 1,400 vehicles. q_{26} also has linear dependence on seven of eight uncertain OD pairs investigated here. q_{26} seems to have a fairly linear dependence on all demands except $d_{10,15}$. However, there exists an evident non-linear relationship between q_{26} and $d_{10,15}$. It should be noted that of the 5 edges originating at node 10, edges 26 and 28 have the highest capacity of 13,916 vehicles each. Edge 27 has a capacity of 10,000 and both edges 29 and 30 have capacities of approximately 5,000 vehicles each. Therefore, it is possible that when a travel large demand such as $d_{10,15}$ is encountered, most of the traffic is routed via routes containing edges 26 and 28 in order to keep edge costs and correspondingly overall network cost low based on equation 4.1. This could be an explanation for the non-linear behavior of *preferred* edge 26.

5.2 Polynomial Chaos Expansion

The original problem was 64 dimensional and required a large number of realizations to be drawn in order to obtain any meaningful statistical inferences about the traffic volume on a link using the Monte Carlo integration technique. This tends to be computationally challenging since a user equilibrium traffic assignment problem needs to solved for each realization set. However, through Figure 4.12 it was demonstrated that most of the uncertainty in the problem is captured by 13 unique dimensions. This is intuitive, since the traffic flow on an edge should only be affected by demands between nodes that is routed through the link. Further, a good surrogate can be constructed using only 300 samples, i.e. approximately 17

times fewer samples as compared to the 500,000 required for Monte Carlo.

Left half of Figure 4.12 depicts amplitudes for all coefficients in a second order PCE of 64 dimensions. The first multi-index represents 0 order for all dimensions, the subsequent 64 represent order 1 for one dimension individually and 0 for the rest, followed by non-linear combinations of multiple dimensions. Therefore, the traffic flow on edge 26 is the resultant of multiple non-linear combinations of demands. The coefficient vector is highly sparse since most coefficients have small amplitudes and will not have significant impact on outcome of the PCE surrogate. After arbitrarily selecting 10^{-2} as a cutoff threshold for amplitude, dimensions represented by "important" coefficients were analyzed which are plotted in the right half of the figure. The dimensions captured represent OD pairs between origins 10 to all destinations $D_{uncertain}$. This is further validation of the intuition that flow on an edge is only affected by uncertain traffic demand routed through it since edge 26 originates from node 10. Dimensions representing node 9, $\{17, 25, 33, 41, 57\}$, as origin have also been sporadically captured. This may be due to the fact that edge 26 terminates at node 9 and for certain values of traffic outflow from node 9, routes between node 10 and $D_{uncertain}$ which include edge 26 may become too expensive thereby affecting flow on it.

Table 4.2 shows that training sample size has the biggest influence on quality of PC surrogate. Expansions created using 100 samples have performed poorly regardless of sampling location and algorithm error threshold parameter values. These expansions have also failed to capture all 8 important dimensions, potential reasons for which are discussed in the following paragraphs. Another noticeable feature is the relatively good performance of all surrogates created using 300 and 500 samples in estimating the mean flow. It should be remembered that numerical values represent vehicle numbers in thousands. Therefore even the worst approximation in case of 500 samples, as provided by set 2 of threshold 10^{-3}, is only off by 7 vehicles. Worst performance in case of 300 samples, again provided by set 2 of threshold 10^{-3}, is off by 6 vehicles. These are reasonably good approximations considering the order of vehicle volume on this edge is in thousands.

Figures 4.13 and 4.14 compare the performance of different training sample sizes and error thresholds used for surrogate construction. 100 samples have performed poorly with both thresholds. A reason for this maybe the fact that the important dimensions captured by the dimensionality reduction algorithm tend to capture 8-9 dimensions of order 2-4. The number of expansion terms in these surrogates exceeds 100 and therefore the least squares system of equations used to obtain these coefficients becomes underdetermined. Sample sizes which result in overdetermined systems, which can be accurately solved in least squares sense, tend to perform better. Once a system has become overdetermined, adding more samples only improves the result marginally which was verified in the case of 300 and 500 samples using

the cross-validation metric values.

There is also the issue of importance of dimension vs. order. Lower error threshold of 10^{-3} results in surrogates of order 3 or 4 but only 8 dimensions for sample sizes 300 and 500 whereas error threshold 10^{-2} results in surrogates of dimension 9, occasionally 10, of maximum order 2. It can be hypothesized that capturing an additional dimension adds more information to the surrogate than a higher order of already captured dimensions does. This is due to the fact that all surrogates of higher threshold outperform their lower threshold counterparts for the sample size and sampling location. However, the error threshold cannot be set arbitrarily large. Doing so will produce garbage and important dimensions will not be captured consistently. This was verified via experimentation but has not been included in the results here.

Chapter 6

Conclusions

6.1 Current Study

Effect of input uncertainties in travel demand on traffic flow within transportation networks was demonstrated. Figure 4.2 shows the distribution of traffic volume on two edges of interest in the benchmark Sioux Falls transportation network. 64 OD pairs were modeled as random inputs with 50% variation about the nominal point estimates obtained from the original data source. Deterministic evaluation of traffic assignment results in point estimates for vehicle volumes. Edges 26 and 32 have nominal traffic flow of 2,603 and 3,556, respectively. In addition to failure in capturing the full extent of flow distributions, these values may also not be the most frequently encountered for these edges.

Smolyak sparse grid sampling approach was demonstrated as a prospective option for stochastic treatment of the traffic assignment problem under travel demand uncertainties. The analytical and computational performance of this technique was compared with the benchmark Monte Carlo sampling approach. Evidence for superior performance of sparse grid interpolation was presented. It was shown that it is possible to recover complete output distributions using as many as 5 times fewer samples than Monte Carlo technique. This translates to significant computational effort savings.

Additionally, the functional relationship of traffic flows on uncertain travel demands inputs was explored. Most edges were found to have linear dependence in case of moderate demand. However, one large capacity edge was found to have non-linear dependence on a travel demand with large variation. Possible reasons for this, with regard to choice of traffic assignment algorithm, were discussed.

It was successfully demonstrated in this work that accurate PC expansion surrogates can be constructed using a small set of samples, which may be obtained from field or synthetically generated based on distribution of traffic demand. The surrogates so constructed are

edge-specific and of lower dimensionality in comparison to the full extent of uncertainty in the problem owing to the iterative greedy algorithm for dimension reduction. These surrogates can then be evaluated at a large number of realization sets in order to fully characterize the output. Any nature of information can then be drawn from the distributions including but not limited to median flow, mean, extremes, and tail probabilities. This will enable planners and engineers to make informed decisions about network characteristics and configurations, consequently leading to optimally constructed networks and reduction in project cost overruns.

6.2 Future Work

The principal contribution of this work was the development of a methodology to analyze approximately real-life scenario traffic volumes in a pragmatically sized network. However, simplification in terms of *partial uncertainty* in travel demand had to be made. This was enforced by a strict limitation the *curse of dimensionality* imposes on any stochastic numerical analysis. With an increase in dimensions, the number of points even in a low order Smolyak sparse grid quickly become too large to avail any significant advantage over the Monte Carlo technique. In case of PCE, creating the measurement matrix becomes a time consuming process. Even the iterative dimension reduction procedure begins to consume a large amount of computational resources since the number of combinations to be tested become large. Yet, a full-sized network for a typical big city containing only the major roads and zonal nodes is sufficiently large to produce aforementioned challenges.

One way to alleviate this problem is to *reduce* the network to the size of Sioux Falls and use the existing methodology. While this might be a valid strategy via a network aggregation model, aggregating uncertainties will prove a challenge. The resultant distribution of travel demand may not be as nicely distributed as a uniform distribution and advanced sampling techniques will have to be employed. The larger issue, however, is the loss of detail. Despite being a major city itself, it is not possible to reduce the road network of every city down to the sketch size of Sioux Falls. Granularity plays a key role since the final application of this analysis technique is in assisting urban planners make decisions about road network configurations.

Second alternative is *dimension reduction*. Instead of reducing the network, it might be possible to reduce the dimensionality of the problem by aggregating uncertainties. Intuitively, when a specific edge is being analyzed, all paths passing through the said edge and originating from a single origin can be grouped. Preliminary tests on this theory were performed and results are presented in Figure 6.1. Based on the plot, it appears that this aggregation

method produces erroneous results for multiple edges perhaps due to simple addition of random variables. However, these exists potential to refine this technique and make it applicable to large networks.

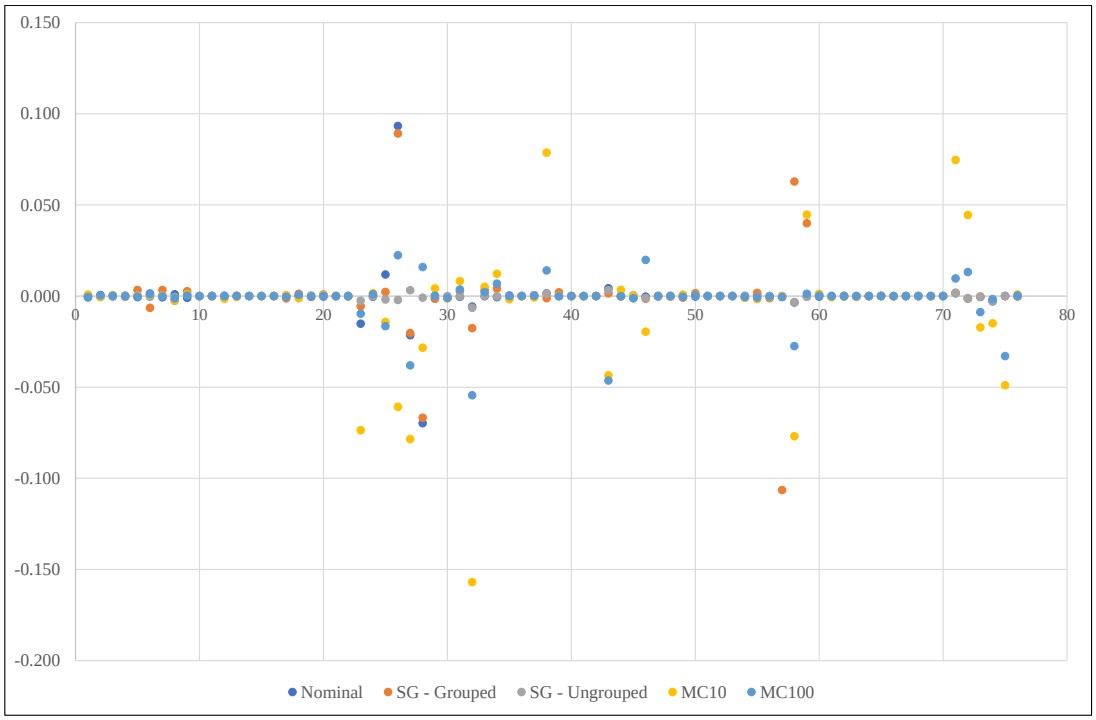

Figure 6.1: Absolute errors in traffic flow estimates obtained using Smolyak sparse grid with path grouping and no grouping, and Monte Carlo with 10 and 100 iterations for all 76 edges in Sioux Falls. Additionally, nominal values with no uncertainty also plotted.

Another direction is correlation between sensitivity of edges to variation in demand and reliability metrics such as edge importance. Calculation of latter for large networks can prove to be a time consuming process which can potentially be sped up by exploiting the reduced dimension strategy for identifying most influential OD pairs.

References

[1] Ralph C Smith. *Uncertainty quantification: theory, implementation, and applications*, volume 12. Siam, 2013.

[2] Ioannis Karatzas and Steven Shreve. *Brownian motion and stochastic calculus*, volume 113. Springer Science & Business Media, 2012.

[3] Peter Eris Kloeden, Eckhard Platen, and Henri Schurz. *Numerical solution of SDE through computer experiments*. Springer Science & Business Media, 2012.

[4] CW Gardiner. Handbook of stochastic methods for physics, chemistry and the natural sciences. *Applied Optics*, 25:3145, 1986.

[5] Bernt Øksendal. *Stochastic differential equations: an introduction with applications*. Springer Science & Business Media, 2003.

[6] Wei-Liem Loh et al. On latin hypercube sampling. *The annals of statistics*, 24(5):2058–2080, 1996.

[7] Michael Stein. Large sample properties of simulations using latin hypercube sampling. *Technometrics*, 29(2):143–151, 1987.

[8] Harald Niederreiter. *Random number generation and quasi-Monte Carlo methods*. SIAM, 1992.

[9] Harald Niederreiter, Peter Hellekalek, Gerhard Larcher, and Peter Zinterhof. *Monte Carlo and quasi-Monte Carlo methods 1996: proceedings of a conference at the University of Salzburg, Austria, July 9-12, 1996*, volume 127. Springer Science & Business Media, 2012.

[10] Bennett L Fox. *Strategies for Quasi-Monte Carlo*, volume 22. Springer Science & Business Media, 1999.

[11] Wing Kam Liu, Ted Belytschko, and A Mani. Probabilistic finite elements for nonlinear structural dynamics. *Computer Methods in Applied Mechanics and Engineering*, 56(1):61–81, 1986.

[12] Wing Kam Liu, Ted Belytschko, and A Mani. Random field finite elements. *International journal for numerical methods in engineering*, 23(10):1831–1845, 1986.

[13] Michael Kleiber and Tran D Hien. *The stochastic finite element method: for use on IBM PC/XT*. Wiley, 1992.

[14] Fumio Yamazaki, Associate Member, Masanobu Shinozuka, and Gautam Dasgupta. Neumann expansion for stochastic finite element analysis. *Journal of Engineering Mechanics*, 114(8):1335–1354, 1988.

[15] Tsuyoshi Takada. Weighted integral method in stochastic finite element analysis. *Probabilistic Engineering Mechanics*, 5(3):146–156, 1990.

[16] George Deodatis. Weighted integral method. i: stochastic stiffness matrix. *Journal of Engineering Mechanics*, 117(8):1851–1864, 1991.

[17] George Deodatis and Masanobu Shinozuka. Weighted integral method. ii: response variability and reliability. *Journal of Engineering Mechanics*, 117(8):1865–1877, 1991.

[18] Dongbin Xiu and George Em Karniadakis. Modeling uncertainty in steady state diffusion problems via generalized polynomial chaos. *Computer methods in applied mechanics and engineering*, 191(43):4927–4948, 2002.

[19] Jun S. Liu. *Monte Carlo strategies in scientific computing*.

[20] F. Nobile, R. Tempone, and C. G. Webster. An Anisotropic Sparse Grid Stochastic Collocation Method for Partial Differential Equations with Random Input Data. *SIAM Journal on Numerical Analysis*, 46(5):2411–2442, jan 2008.

[21] Dongbin Xiu and George Em Karniadakis. Modeling uncertainty in flow simulations via generalized polynomial chaos. *Journal of Computational Physics*, 187(1):137–167, 2003.

[22] Norbert Wiener. The homogeneous chaos. *American Journal of Mathematics*, 60(4):897–936, 1938.

[23] Dongbin Xiu and George Em Karniadakis. The wiener–askey polynomial chaos for stochastic differential equations. *SIAM journal on scientific computing*, 24(2):619–644, 2002.

[24] Roger Ghanem. Scales of fluctuation and the propagation of uncertainty in random porous media. *Water Resources Research*, 34(9):2123–2136, 1998.

[25] Roger Ghanem. Ingredients for a general purpose stochastic finite elements implementation. *Computer Methods in Applied Mechanics and Engineering*, 168(1):19–34, 1999.

[26] Roger Ghanem. Stochastic finite elements with multiple random non-gaussian properties. *Journal of Engineering Mechanics*, 125(1):26–40, 1999.

[27] Pol D Spanos and Roger Ghanem. Stochastic finite element expansion for random media. *Journal of engineering mechanics*, 115(5):1035–1053, 1989.

[28] Christoph Schwab and Radu-Alexandru Todor. Sparse finite elements for elliptic problems with stochastic loading. *Numerische Mathematik*, 95(4):707–734, 2003.

[29] Xiang Ma and Nicholas Zabaras. An adaptive hierarchical sparse grid collocation algorithm for the solution of stochastic differential equations. *Journal of Computational Physics*, 228(8):3084–3113, 2009.

[30] Sergey A Smolyak. Quadrature and interpolation formulas for tensor products of certain classes of functions. In *Dokl. Akad. Nauk SSSR*, volume 4, page 123, 1963.

[31] F. Nobile, R. Tempone, and C. G. Webster. A Sparse Grid Stochastic Collocation Method for Partial Differential Equations with Random Input Data. *SIAM Journal on Numerical Analysis*, 46(5):2309–2345, jan 2008.

[32] Thomas Gerstner and Michael Griebel. Numerical integration using sparse grids. *Numerical Algorithms*, 18(3/4):209–232, 1998.

[33] Volker Barthelmann, Erich Novak, and Klaus Ritter. High dimensional polynomial interpolation on sparse grids. *Advances in Computational Mathematics*, 12(4):273–288, 2000.

[34] Michael Florian and Sang Nguyen. An Application and Validation of Equilibrium Trip Assignment Methods. *Transportation Science*, 10(4):374–390, nov 1976.

[35] Michael. Patriksson. *The traffic assignment problem : models and methods.*

[36] Congressional Budget Office. Public Spending on Transportation and Water Infrastructure, 1956 to 2014. 1956.

[37] Mette K. Skamris. Large Transport Projects:Forecasts versus Actual Traffic and Costs, 1994.

[38] Bent Flyvbjerg, Mette K. Skamris Holm, and Søren L. Buhl. How (In)accurate Are Demand Forecasts in Public works. *Journal of the American Planning Association*, 71(2):131–146, 2005.

[39] Hai Yang and Michael G H. Bell. Models and algorithms for road network design: a review and some new developments. *Transport Reviews*, 18(3):257–278, 1998.

[40] Larry J Leblanc. An algorithm for the discrete network design problem. *Transportation Science*, 9(3):183–199, 1975.

[41] Terry L Friesz, Hsun-Jung Cho, Nihal J Mehta, Roger L Tobin, and G Anandalingam. A simulated annealing approach to the network design problem with variational inequality constraints. *Transportation Science*, 26(1):18–26, 1992.

[42] Omar Ben-Ayed, David E Boyce, and Charles E Blair. A general bilevel linear programming formulation of the network design problem. *Transportation Research Part B: Methodological*, 22(4):311–318, 1988.

[43] Mustafa Abdulaal and Larry J LeBlanc. Continuous equilibrium network design models. *Transportation Research Part B: Methodological*, 13(1):19–32, 1979.

[44] Agachai Sumalee, David Watling, and Shoichiro Nakayama. Reliable network design problem: case with uncertain demand and total travel time reliability. *Transportation Research Record: Journal of the Transportation Research Board*, (1964):81–90, 2006.

[45] David Z. W. Wang and Dong-Fan Xie. Reliable transportation network design considering uncertain demand variability. *International Journal of Sustainable Transportation*, 10(8):752–763, 2016.

[46] Bruce N Janson. Dynamic traffic assignment for urban road networks. *Transportation Research Part B: Methodological*, 25(2):143–161, 1991.

[47] DSATURN Van Vliet. Saturn-a modern assignment model. *Traffic Engineering & Control*, 23(HS-034 256), 1982.

[48] Robert B Dial. A probabilistic multipath traffic assignment model which obviates path enumeration. *Transportation research*, 5(2):83–111, 1971.

[49] William HK Lam and Hai-Jun Huang. A combined trip distribution and assignment model for multiple user classes. *Transportation Research Part B: Methodological*, 26(4):275–287, 1992.

[50] Kara Maria Kockelman. the Propagation of Uncertainty Through Travel Demand Models : an. pages 1–25, 2002.

[51] Satish V. Ukkusuri, Tom V. Mathew, and S. Travis Waller. Robust transportation network design under demand uncertainty. *Computer-Aided Civil and Infrastructure Engineering*, 22(1):6–18, 2007.

[52] Michael D Meyer and Eric J Miller. *Urban transportation planning: a decision-oriented approach*. 1984.

[53] F. Leurent. Sensitivity and error analysis of the dual criteria traffic assignment model. *Transportation Research Part B: Methodological*, 32(3):189–204, 1998.

[54] Stella Dafermos. Traffic Equilibrium and Variational Inequalities. *Transportation Science*, 14(1):42–54, 1980.

[55] Hsun-Jung Cho, Tony E Smith, and Terry L Friesz. A reduction method for local sensitivity analyses of network equilibrium arc flows. *Transportation Research Part B: Methodological*, 34(1):31–51, 2000.

[56] G.W. Wasilkowski and H. Wozniakowski. Explicit Cost Bounds of Algorithms for Multivariate Tensor Product Problems. *Journal of Complexity*, 11(1):1–56, mar 1995.

[57] Hermann Engels. Numerical quadrature and cubature. 1980.

[58] Thomas F. Coleman and Yuying Li. A Reflective Newton Method for Minimizing a Quadratic Function Subject to Bounds on Some of the Variables. *SIAM Journal on Optimization*, 6(4):1040–1058, nov 1996.

[59] Nick Gould and Philippe L Toint. Digital Object Identifier (Preprocessing for quadratic programming. *Math. Program., Ser. B*, 100:95–132, 2004.

[60] Philip E. Gill, Walter. Murray, and Margaret H. Wright. *Practical optimization*. Academic Press, 1981.

[61] Nicholas Metropolis and S Ulam. The Monte Carlo Method. *Journal of the American Statistical Association*, 44(247):335–341, 1949.

[62] Zdravko I Botev, Joseph F Grotowski, Dirk P Kroese, et al. Kernel density estimation via diffusion. *The Annals of Statistics*, 38(5):2916–2957, 2010.

[63] Andreas Klimke and Barbara Wohlmuth. Algorithm 847: spinterp: Piecewise multilinear hierarchical sparse grid interpolation in MATLAB. *ACM Transactions on Mathematical Software*, 31(4), 2005.

[64] Andreas Klimke. Sparse Grid Interpolation Toolbox – user's guide. Technical Report IANS report 2007/017, University of Stuttgart, 2007.

[65] Negin Alemazkoor and Hadi Meidani. Divide and conquer: An incremental sparsity promoting compressive sampling approach for polynomial chaos expansions. *Computer Methods in Applied Mechanics and Engineering*, 318:937–956, 2017.

[66] Larry J. LeBlanc, Edward K. Morlok, and William P. Pierskalla. An efficient approach to solving the road network equilibrium traffic assignment problem. *Transportation Research*, 9(5):309–318, oct 1975.

[67] Chaisak Suwansirikul, Terry L Friesz, and Roger L Tobin. Equilibrium decomposed optimization: a heuristic for the continuous equilibrium network design problem. *Transportation science*, 21(4):254–263, 1987.

[68] Edward K Morlok. *Development and application of a highway network design model*. Federal Highway Administration, 1973.

Appendix A

Complete Sparse Grid Numerical Results

A complete list of numerical results for all edges obtained using the Smolyak sparse grid procedure have been provided here. While the time ratio for a large number of edges is quite small, meaning Monte Carlo outperforms the Smolyak sparse Grid method, attention must be given to the fact that network level decisions cannot be made until information about all components is available. Further, a large proportion of these edges do not fall on the probable shortest paths between any of the uncertain origin destination pairs and therefore display extremely low variability in terms of results. Consequently, the Monte Carlo tolerance criterion is reached in less than 100 iterations. A few new terms need to be defined in order to fully understand the data presented in the following table. These are:

$$\text{Monte Carlo estimate}, \theta_{MC} = \frac{1}{M_{mc}} \sum_{j=1}^{M_{mc}} q_{mc}^{(j)} \tag{A.1}$$

$$\text{Percentage Error}, \epsilon_p = \epsilon_{\bar{q},mc}/\theta_{MC} \tag{A.2}$$

Route ID	Origin	Destination	tol_{MC}	θ_{MC}	$\epsilon_{\bar{q},mc}$	ϵ_p	τ
1	1	2	0.004	3.723	0.003	0.002	0.012
2	1	3	0.006	5.954	0.000	0.000	0.012
3	2	1	0.0000	0.133	0.000	0.000	73.060
4	2	6	0.004	4.267	0.000	0.000	0.015
5	3	1	0.001	0.661	0.004	0.002	0.050
6	3	4	0.002	1.755	0.010	0.005	0.022
7	3	12	0.001	0.662	0.004	0.002	0.015
8	4	3	0.006	5.592	0.001	0.001	0.022
9	4	5	0.002	2.116	0.002	0.001	0.021

Route ID	Origin	Destination	tol_{MC}	θ_{MC}	$\epsilon_{\bar{q},mc}$	ϵ_p	τ
10	4	11	0.005	5.162	0.000	0.000	0.015
11	5	4	0.0000	0.103	0.000	0.000	70.869
12	5	6	0.007	6.505	0.002	0.001	0.015
13	5	9	0.0000	0.101	0.000	0.000	71.131
14	6	2	0.002	1.897	0.000	0.000	0.017
15	6	5	0.004	3.727	0.000	0.000	0.014
16	6	8	0.003	2.736	0.000	0.000	0.015
17	7	8	0.012	11.687	0.004	0.002	0.014
18	7	18	0.002	1.621	0.001	0.001	0.013
19	8	6	0.007	6.710	0.000	0.000	0.013
20	8	7	0.0000	0.321	0.001	0.000	67.280
21	8	9	0.006	5.569	0.000	0.000	0.014
22	8	16	0.006	5.771	0.000	0.000	0.015
23	9	5	0.010	10.438	0.012	0.006	12.787
24	9	8	0.007	6.681	0.019	0.009	0.013
25	9	10	0.0010	0.845	0.003	0.001	48.739
26	10	9	0.003	2.691	0.084	0.042	65.001
27	10	11	0.014	14.357	0.024	0.012	2.694
28	10	15	0.014	13.756	0.080	0.040	21.557
29	10	16	0.011	10.801	0.014	0.007	0.020
30	10	17	0.008	7.969	0.002	0.001	0.014
31	11	4	0.005	4.600	0.016	0.008	0.026
32	11	10	0.004	3.552	0.015	0.007	70.057
33	11	12	0.008	7.679	0.001	0.001	0.012
34	11	14	0.009	8.768	0.008	0.004	0.015
35	12	3	0.004	3.811	0.002	0.001	0.013
36	12	11	0.008	8.397	0.000	0.000	0.013
37	12	13	0.003	3.191	0.001	0.000	0.013
38	13	12	0.005	4.834	0.007	0.003	40.188
39	13	24	0.011	11.111	0.002	0.001	0.013
40	14	11	0.006	5.924	0.000	0.000	0.013
41	14	15	0.005	5.232	0.000	0.000	0.014
42	14	23	0.004	4.354	0.000	0.000	0.013
43	15	10	0.005	4.760	0.010	0.005	21.072
44	15	14	0.009	8.610	0.010	0.005	0.013

Route ID	Origin	Destination	tol_{MC}	θ_{MC}	$\epsilon_{\bar{q},mc}$	ϵ_p	τ
45	15	19	0.001	1.030	0.002	0.001	0.797
46	15	22	0.009	9.005	0.003	0.002	1.669
47	16	8	0.008	7.801	0.000	0.000	0.012
48	16	10	0.01	10.424	0.000	0.000	0.015
49	16	17	0.01	9.948	0.001	0.001	0.012
50	16	18	0.001	0.542	0.003	0.002	0.015
51	17	10	0.008	7.670	0.000	0.000	0.013
52	17	16	0.01	9.614	0.000	0.000	0.013
53	17	19	0.008	8.455	0.000	0.000	0.013
54	18	7	0.001	1.385	0.000	0.000	0.109
55	18	16	0.002	2.175	0.004	0.002	0.020
56	18	20	0.002	1.614	0.001	0.000	0.013
57	19	15	0.0000	0.348	0.107	0.053	70.990
58	19	17	0.007	6.833	0.062	0.031	7.952
59	19	20	0.007	6.900	0.046	0.023	2.499
60	20	18	0.0000	0.368	0.001	0.001	72.754
61	20	19	0.008	7.870	0.000	0.000	0.013
62	20	21	0.006	5.716	0.000	0.000	0.013
63	20	22	0.006	6.287	0.000	0.000	0.013
64	21	20	0.004	4.115	0.000	0.000	0.013
65	21	22	0.001	1.370	0.000	0.000	0.013
66	21	24	0.007	6.615	0.000	0.000	0.012
67	22	15	0.005	4.766	0.000	0.000	0.014
68	22	20	0.006	6.360	0.000	0.000	0.013
69	22	21	0.007	6.805	0.000	0.000	0.013
70	22	23	0.009	8.909	0.000	0.000	0.014
71	23	14	0.006	6.096	0.009	0.005	2.316
72	23	22	0.007	7.166	0.007	0.004	1.559
73	23	24	0.003	2.695	0.005	0.003	41.141
74	24	13	0.005	5.020	0.001	0.001	5.633
75	24	21	0.003	3.377	0.002	0.001	19.129
76	24	23	0.0000	0.182	0.000	0.000	66.593

Appendix B

PCE Cross Validation Histograms

Comparison between actual traffic volume distributions for edge 26 and estimates obtained using PCE surrogates created using different combinations of error thresholds, and training sample locations and sizes have been presented in the form of histograms. Blue bars in all figures represent the actual values and orange bars represent the estimates. Overlap between the two, represented by a brown shade illustrates the accuracy of prediction. A total of 100 testing locations were considered.

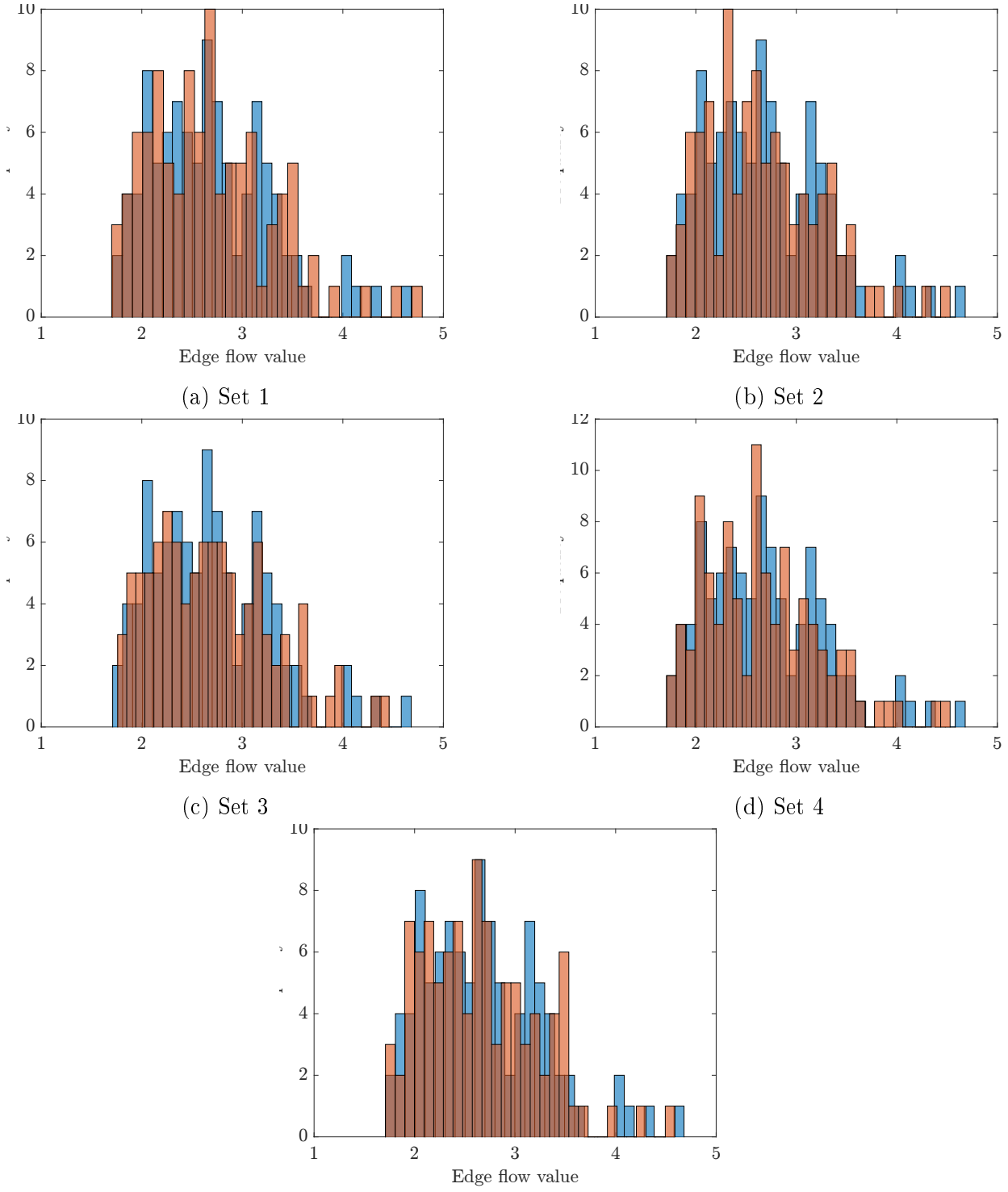

(a) Set 1

(b) Set 2

(c) Set 3

(d) Set 4

(e) Set 5

Figure B.1: Histogram comparing true vehicle volumes with estimated volumes obtained using reduced dimension PCE surrogates with error threshold 10^{-2} and 5 different sampling locations for training data of size 500.

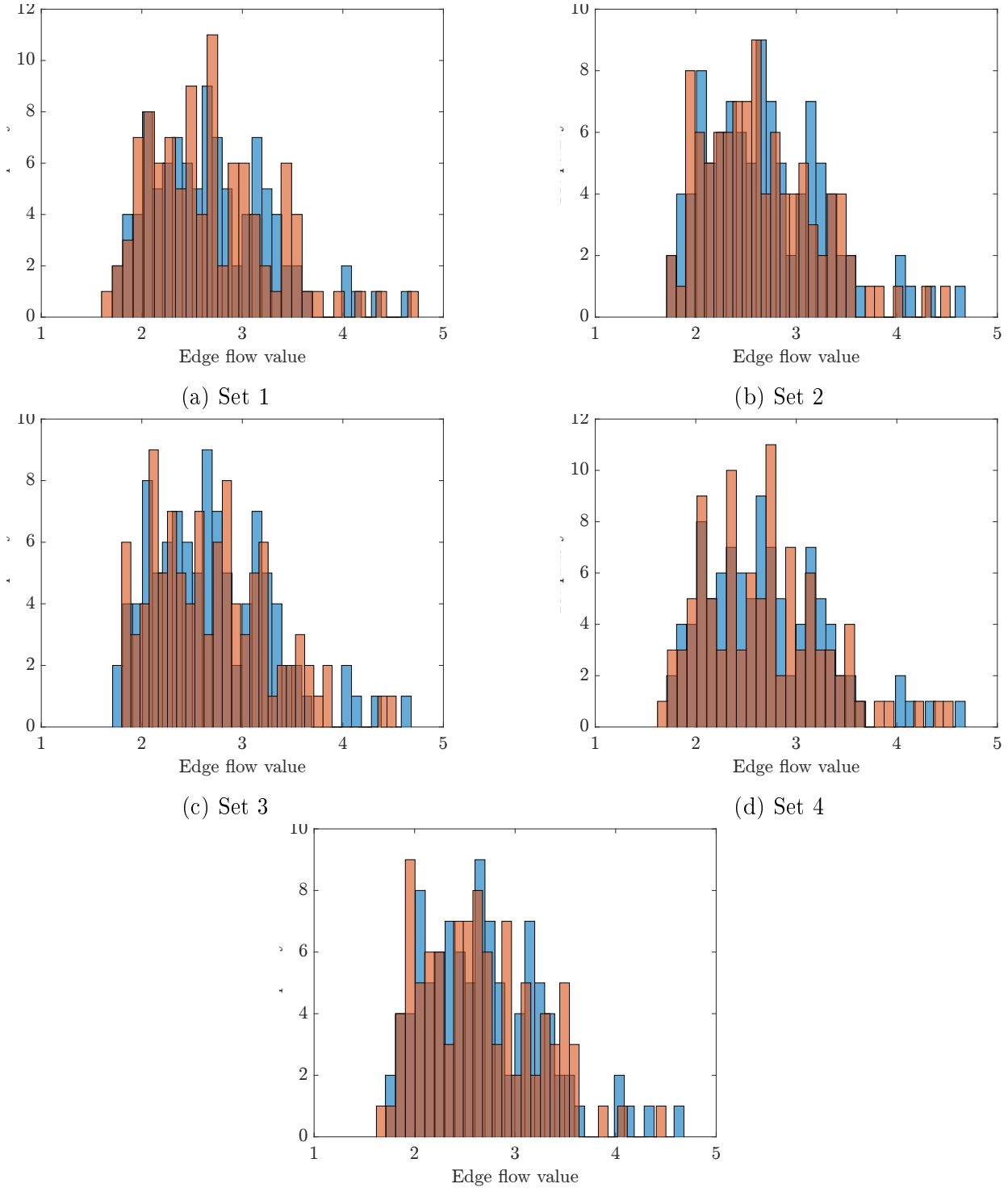

(a) Set 1

(b) Set 2

(c) Set 3

(d) Set 4

(e) Set 5

Figure B.2: Histogram comparing true vehicle volumes with estimated volumes obtained using reduced dimension PCE surrogates with error threshold 10^{-2} and 5 different sampling locations for training data of size 300.

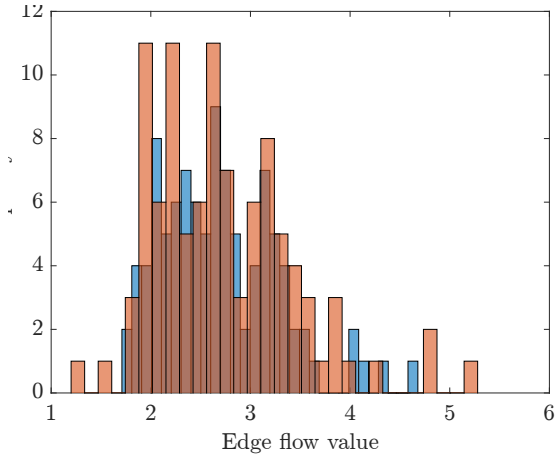

(a) Set 1

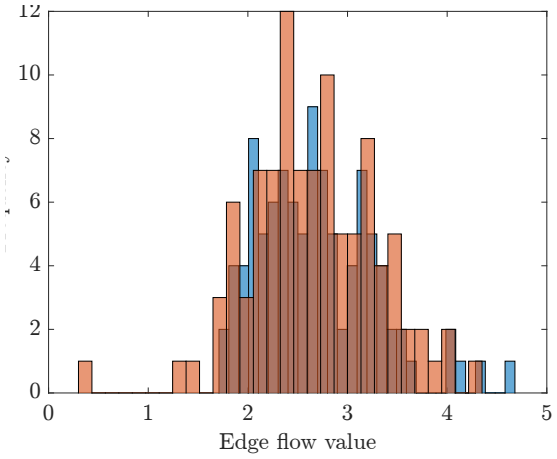

(b) Set 2

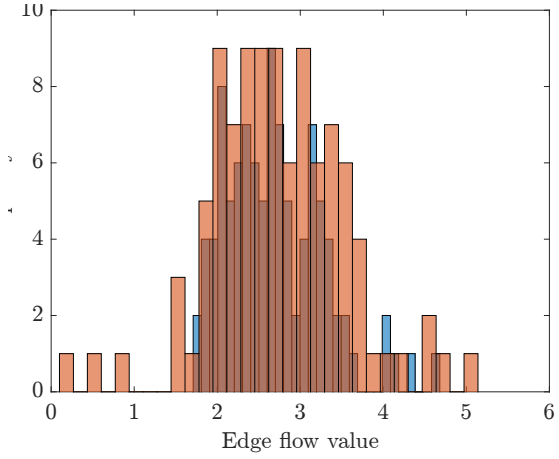

(c) Set 3

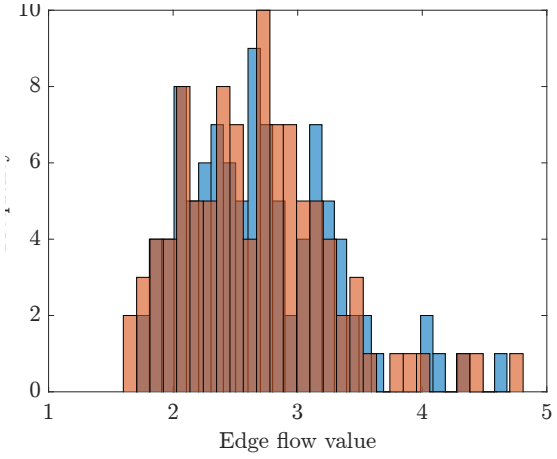

(d) Set 4

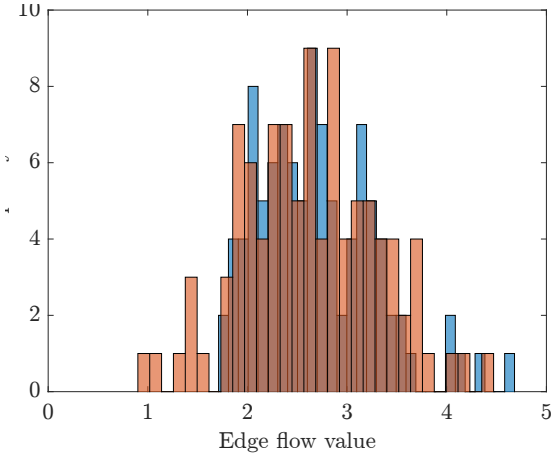

(e) Set 5

Figure B.3: Histogram comparing true vehicle volumes with estimated volumes obtained using reduced dimension PCE surrogates with error threshold 10^{-2} and 5 different sampling locations for training data of size 100.

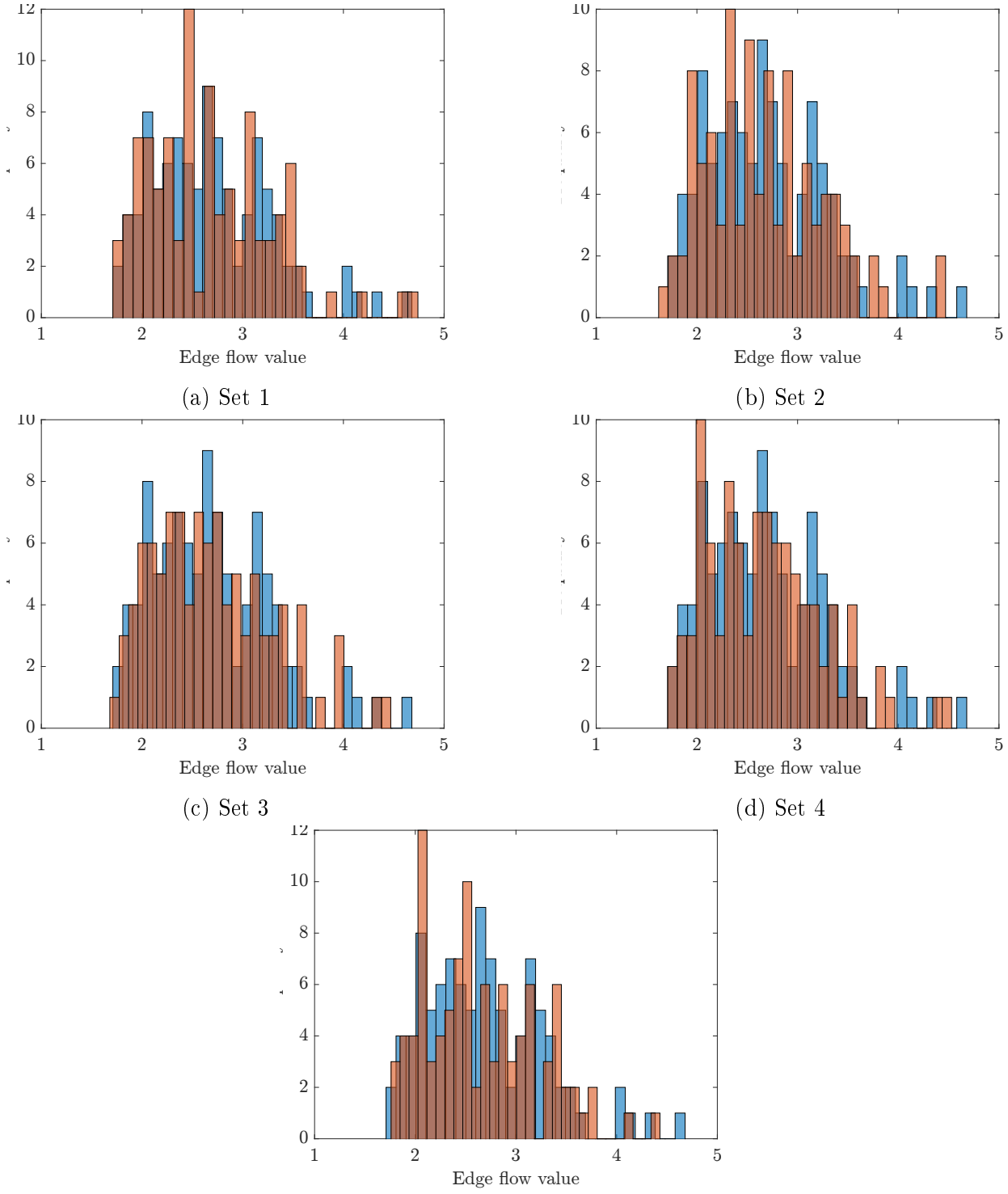

(a) Set 1

(b) Set 2

(c) Set 3

(d) Set 4

(e) Set 5

Figure B.4: Histogram comparing true vehicle volumes with estimated volumes obtained using reduced dimension PCE surrogates with error threshold 10^{-3} and 5 different sampling locations for training data of size 500.

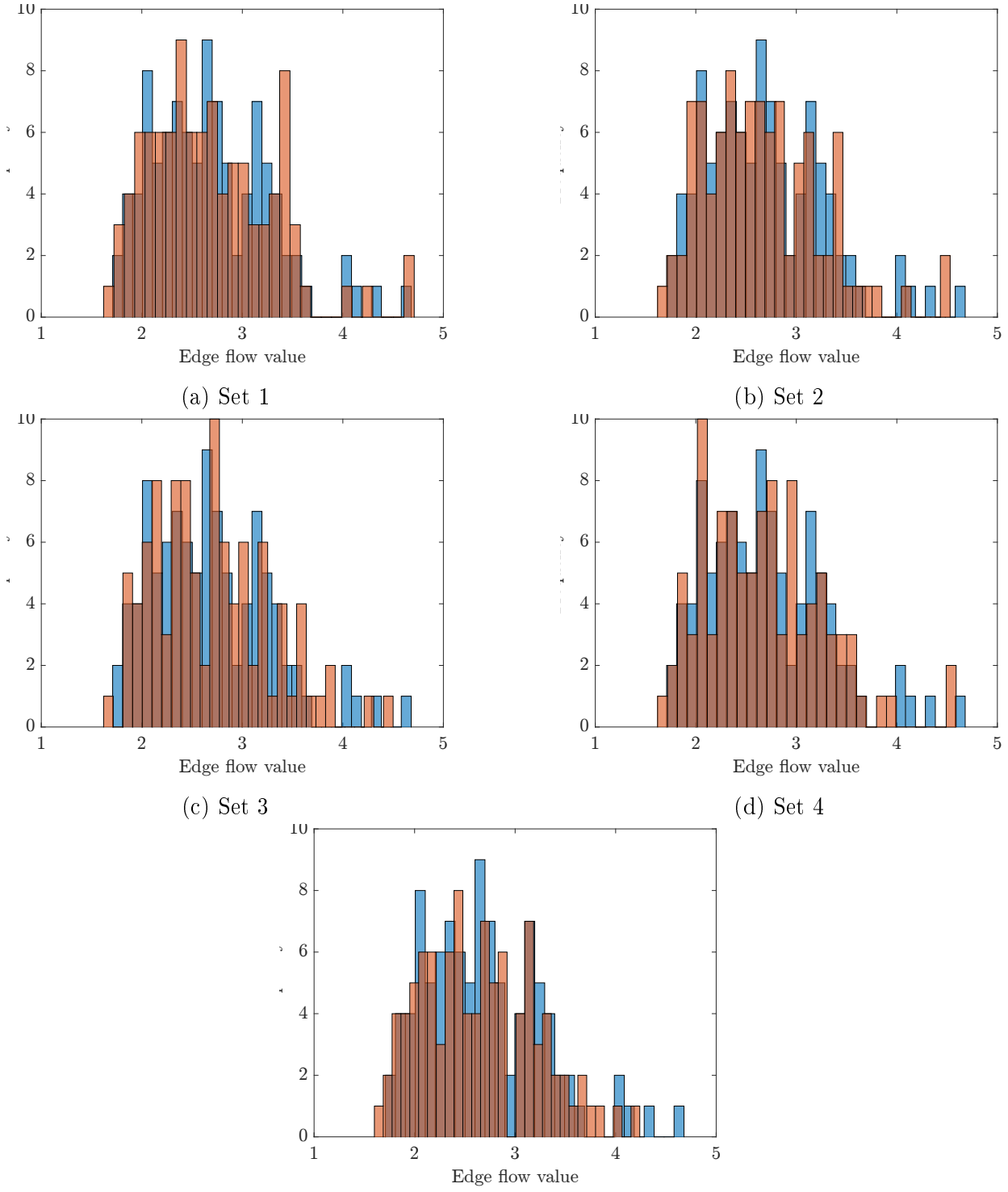

(a) Set 1

(b) Set 2

(c) Set 3

(d) Set 4

(e) Set 5

Figure B.5: Histogram comparing true vehicle volumes with estimated volumes obtained using reduced dimension PCE surrogates with error threshold 10^{-3} and 5 different sampling locations for training data of size 300.

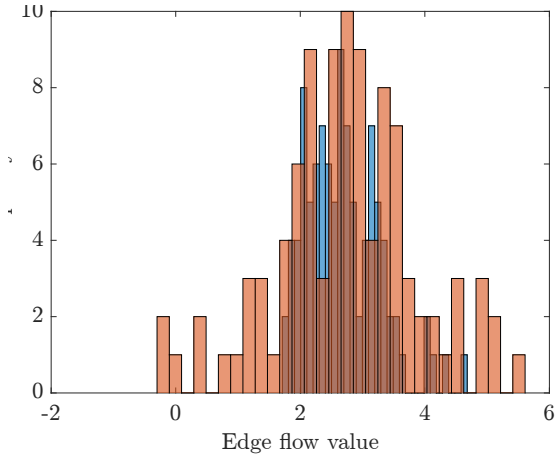

(a) Set 1

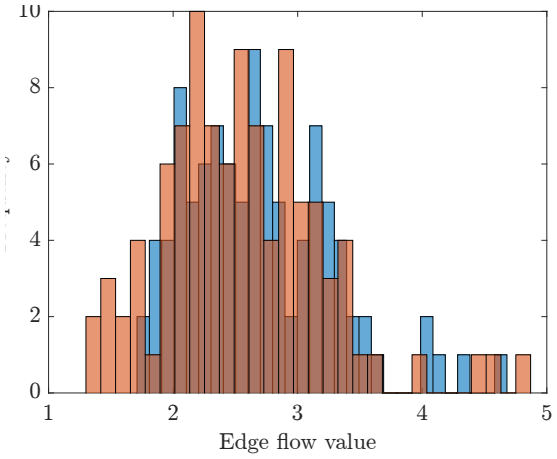

(b) Set 2

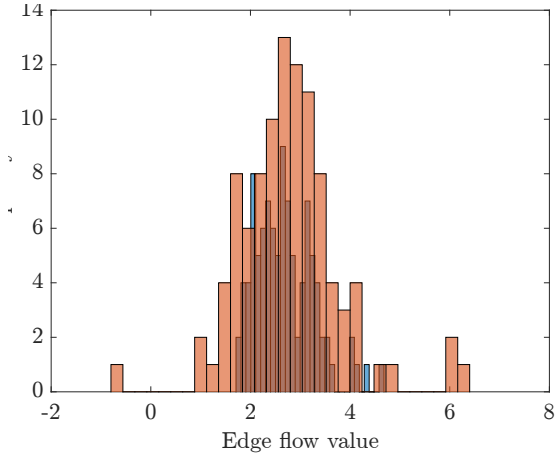

(c) Set 3

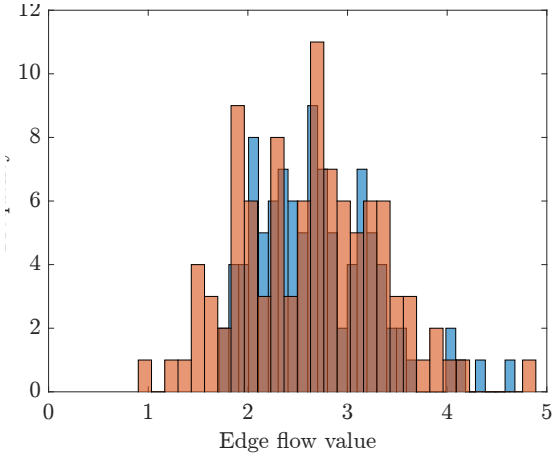

(d) Set 4

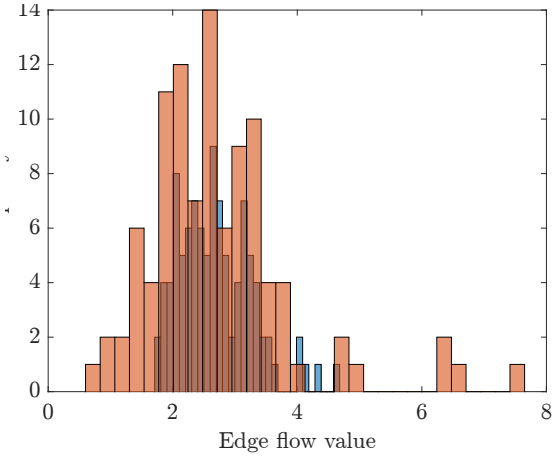

(e) Set 5

Figure B.6: Histogram comparing true vehicle volumes with estimated volumes obtained using reduced dimension PCE surrogates with error threshold 10^{-3} and 5 different sampling locations for training data of size 100.